Binary Passive Element Leg: A Design Framework for a Legged System

A Thesis Presented
by

Daniel Carlson

to

The Department of Mechanical and Industrial Engineering

in partial fulfillment of the requirements
for the degree of

Master of Science

in

Mechanical Engineering

Northeastern University
Boston, Massachusetts

April 2024

To my family.

Contents

List of Figures iv

List of Tables vi

List of Acronyms vii

Acknowledgments viii

Abstract ix

1 Introduction 1
- 1.1 Quick State of the Art Review of Leg Model Design . . . 2
  - 1.1.1 Spring Loaded Inverted Pendulum . . . 2
  - 1.1.2 Series Elastic Actuation . . . 2
  - 1.1.3 2xSeries Elastic Actuation . . . 4
  - 1.1.4 Parallel Elastic Actuation . . . 5
  - 1.1.5 Series-Parallel Elastic Actuation . . . 6
  - 1.1.6 Damper Actuator SLIP . . . 6
  - 1.1.7 Proprioceptive Actuation . . . 6
- 1.2 Quick State of the Art Review of Leg Hardware Design . . . 7
  - 1.2.1 Prismatic Legs . . . 7
  - 1.2.2 Articulated Legs . . . 8
- 1.3 Quick State of the Art Review of Leg Architectures . . . 10
- 1.4 Project Goals . . . 11

2 Design Overview 12
- 2.1 Overview of Current Harpy Design . . . 12
  - 2.1.1 Current Harpy Leg Design . . . 13
  - 2.1.2 Current Harpy Actuator Design . . . 14
- 2.2 Overview of the Binary Passive Element Leg Design . . . 16
  - 2.2.1 Reduced Order Model . . . 16
  - 2.2.2 Kinematic Design . . . 18
  - 2.2.3 Actuator Design . . . 21

3 Variable Selection **22**
3.1 Shock Absorber Selection . . . 22
3.1.1 Theory . . . 22
3.1.2 Analysis for Harpy Leg . . . 22
3.2 Limb Length Selection . . . 23
3.2.1 Theory . . . 23
3.2.2 Analysis for Harpy Leg . . . 24
3.3 Spring Constant Selection . . . 25
3.3.1 Theory . . . 25
3.3.2 Analysis for Harpy Leg . . . 27
3.4 Damping Constant Selection . . . 28
3.4.1 Theory . . . 28
3.4.2 Analysis for Harpy Leg . . . 29

4 Hardware Design **33**
4.1 Actuator Design . . . 33
4.2 Knee Design . . . 35
4.2.1 Knee Spring Design . . . 35
4.3 Foot Design . . . 36
4.3.1 Foot-Shock Interaction . . . 36
4.4 Shock Absorber Design . . . 37
4.5 Complete System . . . 39

5 Simscape Models **41**
5.1 BPE Model Implementation . . . 41
5.2 Jumping Model . . . 42
5.3 Falling Model . . . 44
5.4 Damper Solver Model . . . 48
5.5 Torque Solver Model . . . 48

6 Results **52**
6.1 Falling Simulation . . . 52
6.2 Jumping Simulation . . . 54

7 Conclusion **59**
7.1 Future Work . . . 60

Bibliography **61**

List of Figures

1.1 Various legged system reduced order models. 3
1.2 SLIP reduced order model. 4
1.3 ANYmal quadrupedal robot[1]. 4
1.4 WANDERER bipedal robot[2]. 5
1.5 Prismatic leg implementation on Raibert's hopping robot[3]. 8
1.6 Motorized screw prismatic leg implementation in ARL Monopod II.[4] 9
1.7 TITAN-XII quadrupedal robot[5]. 9
1.8 ATRIAS bipedal robot[6]. 10
1.9 Sprawling and mammal type leg architectures. 11

2.1 Current Harpy platform[7]. 13
2.2 Schuebeler DS-38 AXI HDS 14
2.3 Current Harpy leg. 15
2.4 Current Harpy actuator. 16
2.5 RMB20 encoder module [8] 17
2.6 T-motor Antigravity 4006 [9] 17
2.7 BPE reduced order model. 19
2.8 BPE kinematic configuration. 19
2.9 Five bar linkage example task space. 20

3.1 Ideal shock absorber force vs stroke position curve[10]. 23
3.2 ENIDINE ECO 220 impact velocity vs energy per cycle curve[11]. 24
3.3 Geometric configurations solved to determine limb lengths. 25
3.4 Model BPE leg task space. 26
3.5 5 Bar Force Body Diagram where F_{xlm}, F_{ylm}, F_{xrm}, F_{yrm}, M_{lm}, M_{rm}, M_{lk}, M_{rk}, F_{mass} are the left motor reaction force in the X, the left motor reaction force in the Y, the right motor reaction force in the X, the right motor reaction for in the Y, the moment applied by the left actuator, the moment applied by the right actuator, the moment applied by the left knee spring, the moment applied by the right knee spring, and the ground reaction force respectively. 30
3.6 Harpy BPE leg walkable regions of the task space. 31
3.7 Spring energy cost curve. 31
3.8 Spring constant analysis results from Simulink. 32

3.9 Damping constant analysis results from Simulink. 32

4.1 Current Harpy actuator and new BPE leg actuator comparison. 34
4.2 BPE knee assembly. 35
4.3 BPE foot assembly. 37
4.4 Shock absorber relative to task space. 38
4.5 Shock absorber mount assembly. 39
4.6 Final leg render in both extended and compressed configurations. 40

5.1 Simscape model overview. 42
5.2 Left leg model with added shock extrusion body. 43
5.3 Jumping simulator actuator model. 45
5.4 Jumping simulator shock absorber model. 46
5.5 Falling simulator full model. 47
5.6 Falling simulator shock absorber model. 49
5.7 Damper analysis model. 50
5.8 Torque analysis model. 51

6.1 Falling simulation motion diagram. 53
6.2 Falling simulation actuator torque vs time graph. 54
6.3 Falling simulation GRF vs time. 55
6.4 Falling simulation actuator position vs time graph. 55
6.5 Jumping simulation motion diagram. 56
6.6 Jumping simulation body position vs time graph. 56
6.7 Jumping simulation actuator torque vs time graph. 57
6.8 Jumping simulation GRF vs time graph. 58
6.9 Jumping simulation position vs time graph. 58

List of Tables

2.1 Schuebeler DS-38 AXI HDS EDF with HET 700-68-1400 motor specifications. . . 14
2.2 Harmonic Drive CSF-11-30-2A-R specifications. 17
2.3 RMB 20 specification. 17
2.4 T-motor Antigravity 4006 specification. 17

3.1 Enidine ECO 220-1 Geometry 23
3.2 Harpy leg design parameters. 25
3.3 Harpy leg limb lengths. 25
3.4 Harpy leg spring design parameters. 28

4.1 BPE actuator components. 33

List of Acronyms

BPE Binary Passive Element

BLDC Brushless DC (direct current) motor.

CAD Computer aided design.

CoT Cost of Transportation

GRF Ground Reaction Force

PEA Parallel Elastic Actuation.

SEA Series Elastic Actuation.

SLIP Spring Loaded Inverted Pendulum

SPEA Series Parallel Elastic Configuration

Acknowledgments

This work was made possible by all those at SiliconSynapse Lab at Northeastern University who assisted me during the process of my thesis. Prof. Alireza Ramezani, my primary adviser, has supported and believed in me from the very first day of my graduate studies. He has been instrumental in guiding and challenging me throughout my research career, in addition to giving me the opportunity to work on extremely interesting and exciting projects. I would also like to thank all of my lab mates, including Shreyansh, Kaushik, Kruthica, Aditya, and Adarsh for their help with brainstorming, design, simulation, and consistent encouragement. I would also like to thank Prof. Rifat Sipahi serving as my mechanical engineering department co-adviser and thesis reader. Finally, none of this would be possible without the support of my parents and my brother. Throughout my life, they have always pushed me to be better and been behind me every step of the way for all the things I've wanted to achieve.

Abstract

Binary Passive Element Leg: A Design Framework for a Legged System

by

Daniel Carlson

Master of Science in Mechanical Engineering

Northeastern University, April 2024

Dr. Alireza Ramezani, Adviser

Legged robots are a form of advanced robotic platform that use robotic legs to navigate rough and unknown terrain. To push legged robotics even further, multimodal robotic systems have been developed that can not only walk but fly as well. However, common leg designs for these systems have not pushed the limits of passive elements to achieve system objectives. The development of the binary passive element robotic leg allows the robotic system to have two sets of passive elements that can dynamically change the the effective passive element constants. This enables use cases such as using strong passive elements for energy dissipation due to a fall, while allowing weaker, tuned passive elements to be used during normal walking operations. This thesis explores the design motivation behind the binary passive element leg along with the analytical techniques to develop a binary passive element leg to achieve a wide variety of system objectives. Finally, it designs both the system parameters and hardware for a binary passive element leg that can be implemented on Northeastern's Harpy platform, a bipedal and multimodal robotic system.

Chapter 1

Introduction

Compliance and damping are evidently crucial in legged locomotion. Simplified models like the Spring-Loaded Inverted Pendulum (SLIP) model have unveiled significant insights into how animals, particularly birds, utilize damping and compliance within their musculoskeletal systems to enhance energy efficiency and stability during locomotion. Beyond mere efficiency, compliance is pivotal for agile maneuvers in birds. For example, widowbirds adeptly coordinate their legs and wings to execute high jumps. Within a widowbird's legs, compliant tendons absorb substantial impact loads upon touchdown at the conclusion of jumps. Legged robots, varying in size and actuator types, have gleaned inspiration from animal leg morphology. However, unlike the adaptable compliance and damping inherent in biological skeletal structures, engineered legged robots typically possess fixed characteristics for compliance and damping. While endeavors to achieve adaptive and virtual stiffness-damping characteristics in task space through closed-loop feedback (impedance control) are common and successful, hardware structures exhibiting multi-phase behavior are less explored due to design complexities. In such designs, a significant challenge often encountered is isolating damping and stiffness terms from other design parameters (e.g., kinematic characteristics) without deviating from nominal motions. This chapter will initially overview state-of-the-art leg designs based on hardware design principles. Subsequently, two mainstream models employed in parametrized hardware design for legged systems will be briefly examined. Finally, the Chapter will outline its primary motivation, objectives, and contributions.

1.1 Quick State of the Art Review of Leg Model Design

When designing the leg for a legged robotic system, Rezazadeh et al. lays out a three step plan in ”Robotic Leg Design: A Constructive Framework”[12]. These three steps are template, mechanism and actuators. The template step consists of defining the reduced order model that will be used to inform the creation of a mechanical system in the following steps of this process. The purpose of the reduced order model is to ”capture the unique and dominating characteristics of these systems” without getting slowed down by mechanical implementation. The following sections will discuss various reduced order models that have been used or are currently being used by state-of-the-art robotic systems. A complied image of all the discussed reduced order models can be found in

1.1.1 Spring Loaded Inverted Pendulum

One of the first widely used reduced order models is called the Spring Loaded Inverted Pendulum, or SLIP, model. The model consists of a spring attached to a point mass as seen in Fig. 1.2. The model features a rotary actuator as its single control control input allowing control over the angle of the spring relative to the ground. This simple model is able to reproduce the motion and dynamics of walking bodies and has been widely used and adapted for all types of legged robotic systems.

1.1.2 Series Elastic Actuation

While the simplicity of the SLIP model relative to its accuracy in reproducing a walking gait has made it very popular in legged robotic systems, subsequent models have opted to include more controllable elements. In particular, many models have added an actuator in the lengthwise direction of the model allowing additional control of the leg end position and force. With the combination of actuators and springs, a much larger variety of reduced order models can be constructed.

The first of these is the series elastic actuation, or SEA, model seen in Fig. 1.1a. This model continues with the single spring from the SLIP model but includes a single actuator in series with the elastic element i.e. the spring. By putting the spring in series with the actuator the model gains two advantages. First, the actuator becomes isolated from impulse shock forces applied at the leg end and second the required maximum motor speed is reduced for some movements[13][14].

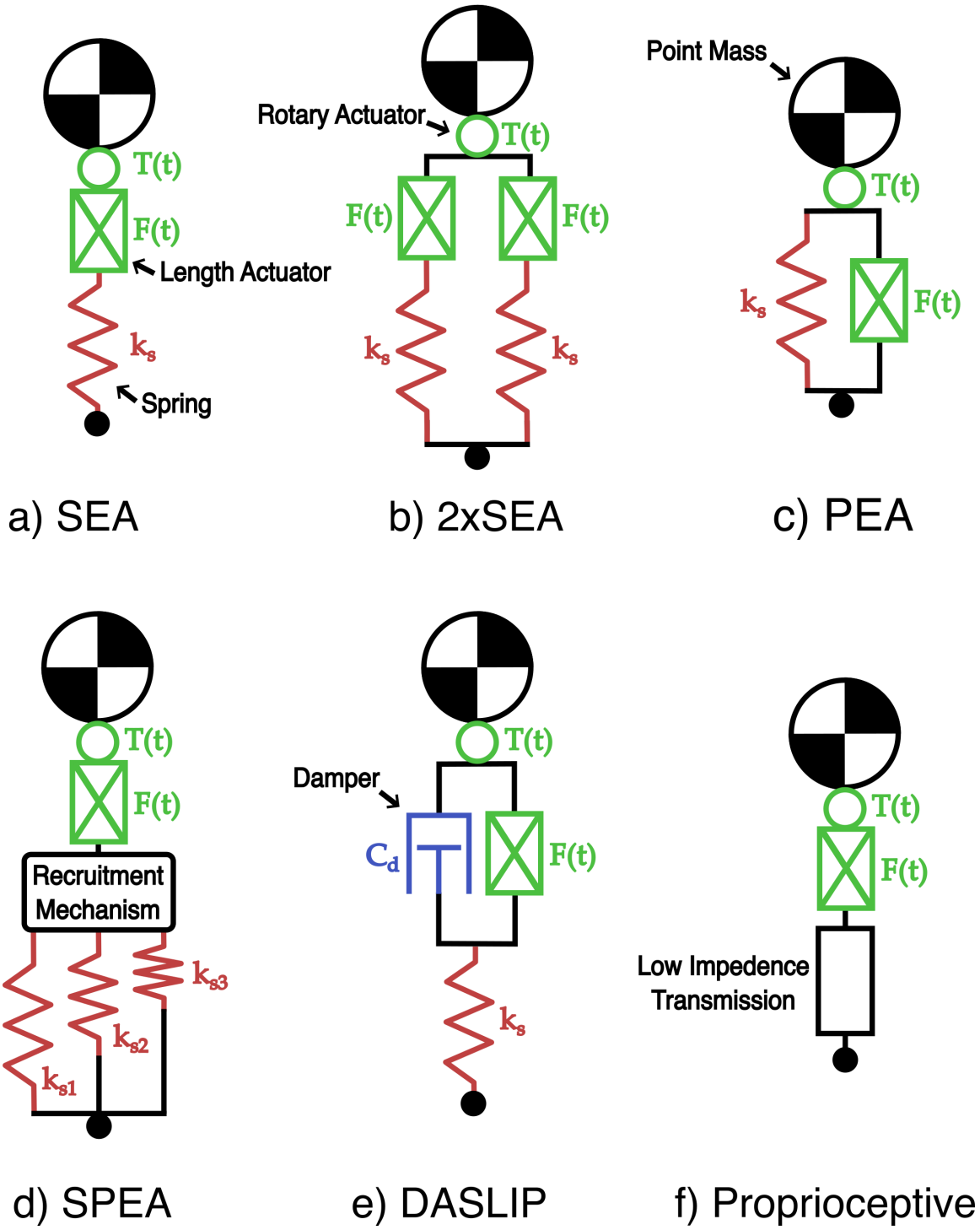

Figure 1.1: Various legged system reduced order models.

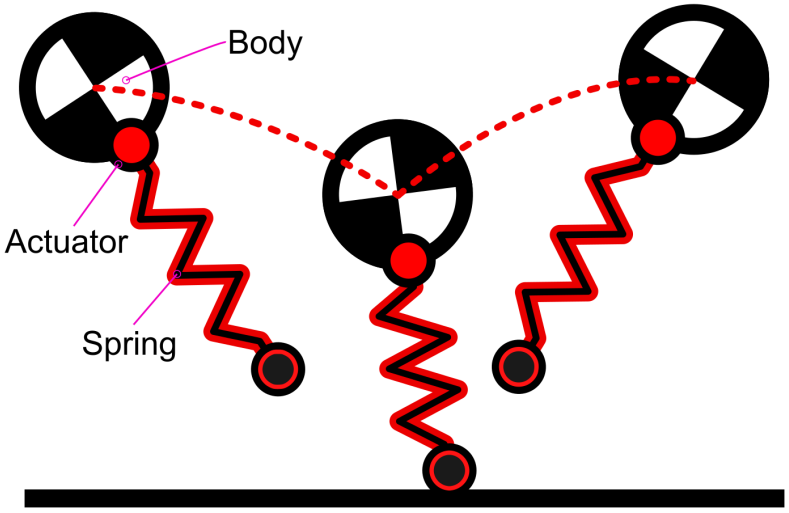

Figure 1.2: SLIP reduced order model.

Figure 1.3: ANYmal quadrupedal robot[1].

The SEA model has proved very popular and has been implemented in robotic systems such as ANYmal[1], a quadrupedal robot developed at ETH Zurich that can be found in Fig. 1.3. ANYmal utilizes the leg end compliance in its motor outputs to achieve improved leg end force control and increased energy recovery. It achieves this improved leg end force control by measuring the deflection of its elastic element, a common practice for SEA model force control

1.1.3 2xSeries Elastic Actuation

While the SEA model has been widely used, some robotic systems require additional control inputs to achieve a desired output. This problem led to the use of a 2xSEA model in the

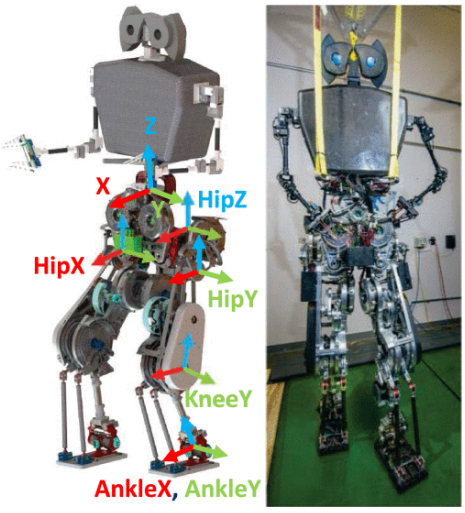

Figure 1.4: WANDERER bipedal robot[2].

paper ”A comparison of parallel- and series elastic elements in an actuator for mimicking human ankle joint in walking and running”[13]. This model features two SEA configurations in parallel as seen in Fig. 1.1b. Gimmer et al. found that the complex movement of a human ankle joint was difficult to reproduce for single actuator models and that the use of two actuators as seen in the 2xSEA model allowed the system to more accurately reproduce desired ankle movement.

1.1.4 Parallel Elastic Actuation

Besides the SEA model, the other configuration available with a single spring and a single actuator is the parallel elastic actuator or PEA configuration. In this configuration, the actuator and elastic element are placed in parallel allowing the actuator direct control over the leg end position as seen in Fig. 1.1c. This leads to a reduction in the peak power and peak torque requirements for the motors to achieve the same outputs as the SEA configuration[15]. This configuration also allows for spring recruitment to increase maximum force output in specific maneuvers.

In the bipedal robot WANDERER seen in Fig. 1.4, a PEA model was utilized in a novel approach to actuator design[2]. WANDERER implements a parallel elastic elements in its hip and ankle actuators to reduce cost of transportation and reduce peak motor torques. The reduction in peak torques allows the motors to be scaled and designed to operate at their most efficient torques and reduce the I^2R losses in the actuators. Without the PEA model, the required torques would have been too large to properly scale the actuators in a reasonable packaging for a humanoid robot.

1.1.5 Series-Parallel Elastic Actuation

Expanding outside of a single spring model, the SPEA model found in Fig. 1.1d uses multiple springs and a recruitment mechanism to reduce actuator torque requirements across wide actuation ranges[16]. The reduction in actuator torque increases system efficiency and enables larger loads without increasing actuator size. The use of springs in series with the actuator also provides the system with the benefits from an SEA model. The cost of these systems comes with the mechanical complexity and size of the recruitment mechanism.

1.1.6 Damper Actuator SLIP

These robotic systems and many more have implemented SEA and PEA configurations for its actuators in an effort to reduce one of the important characteristics of many robotic systems, the cost of transportation or CoT. CoT is the amount of energy that is required to traverse between two locations. This system quality metric leads to the exclusion of damping elements in many robotic systems as it provides no benefit in reducing the CoT for many systems. However, damping can still play an important role in robotic systems if design objectives do not require the minimization of CoT.

One place that damping can be used effectively to achieving design objectives is when building a robust system. The paper ”A Little Damping Goes a Long Way” by Heim et al[17], analyzes the impact of damping elements placed in parallel with actuation on a SEA system. They called this model the DASLIP model and can be found in Fig. 1.1e.

In this paper, it was found that the inclusion of a damping element in parallel with the actuator improved the systems ability to remain stable when encountering unknown ground height perturbations. This robustness to ground height variations without the need for additional control allows the system to be more robust to falling in difficult terrain and could potentially justify its inclusion in spite of its impact on CoT.

1.1.7 Proprioceptive Actuation

Proprioceptive actuators are very different than the other models that have been discussed so far in that they do not include any elastic elements as seen in Fig. 1.1f[18]. These actuators are designed have extremely reliable and accurate force feedback from the leg end to the actuator by specially designing the gear train and leg. This allows for the removal of torque sensing from the actuator design, reducing mass and improving torque density.

1.2 Quick State of the Art Review of Leg Hardware Design

The next step in the robotic leg design framework is the design of the mechanism or kinematics. With the two forms of actuators being rotary and linear actuators, two leg categories emerged. The first category of legs are called prismatic legs which utilize a single rotary and a linear actuator. Prismatic configurations have been used effectively in a wide variety of robotic systems as will be discussed in this section. The other category of legs are called articulated legs which utilize two rotary actuators. As described in "A brief overview of parallel robots and parallel kinematic machines", the two primary configurations for articulated leg kinematics are parallel and serial configurations[19]. Looking at these two categories, the two actuators can be coupled, known as a parallel configuration, or function independently, known as a serial configuration. These two forms of legged kinematics are the most popular choices when designing legged systems and have been implemented in many robotic systems as will be discussed in this section.

1.2.1 Prismatic Legs

With the creation of the SLIP model for robotic systems, a hardware solution that could implement this model in hardware experiments was needed. This led to the creation of the prismatic leg, a leg that features linear motion along the length of the leg by utilizing a prismatic joint.

1.2.1.1 Pneumatic Prismatic Legs

The first prismatic legs developed attempted to accurately reflect the SLIP model. This led to the implementation of pneumatic prismatic legs, a leg that has no electric actuator based control over the length of the leg. This reflects the spring seen in the SLIP model which does not include any length changing actuators. These systems instead used pneumatics to inject energy to the system such as in Raibert's hopping robot found in Fig. 1.5. These legs also implemented the hip actuator featured in the SLIP model to control the angle of the leg relative to the floor.

1.2.1.2 Motorized Screw Type Prismatic

While the passive prismatic leg along with the SLIP model were able to accurately recreate a walking gait, the need for more control over legged systems and, in the case of a prismatic leg, the length of the leg led to the creation of the motorized screw type prismatic leg. This leg implements the prismatic motion of the earlier leg designs but implements an electric motor with a

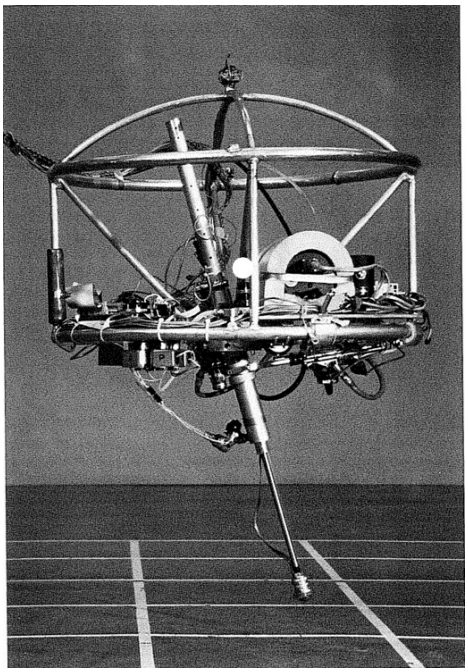

Figure 1.5: Prismatic leg implementation on Raibert's hopping robot[3].

screw enabling the system to have direct control the length of the leg and thus the leg end position. The robot ARL Monopod II seen in Fig. 1.6 implements a screw type prismatic leg[4].

1.2.2 Articulated Legs

As legged system design continued to advance and the use of motors for actuation grew in popularity, articulated leg designs were developed as an alternative to the prismatic leg. Articulated legs feature rotational joints instead of the linear prismatic joint. This allows for more animal like leg dynamics and with proper control can be used to approximate the dynamics of prismatic systems.

With many articulated legs adding additional degrees of freedom to match the versatility of animal limbs, there emerged two primary kinematic configurations for the actuators, those being serial and parallel configurations.

1.2.2.1 Serial Configuration

The serial configuration features the actuators is series where the actuators are not linked together and form an open loop kinematic chain. These manipulators benefit from an increased task space volume and reduced mechanical complexity due to a lack of kinematic couplings.

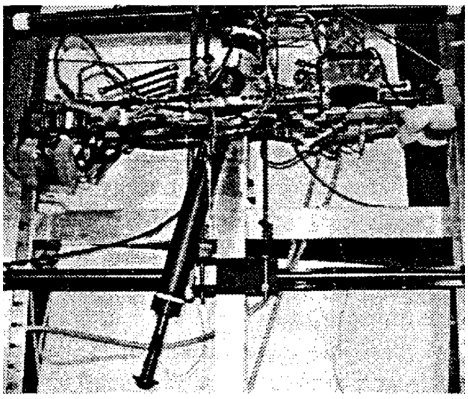

Figure 1.6: Motorized screw prismatic leg implementation in ARL Monopod II.[4]

Figure 1.7: TITAN-XII quadrupedal robot[5].

Many robotic systems have implemented this configuration such as the robot TITAN-XII[5]. TITAN-XII uses a serial configuration but uses a pulley system to move the mass of the knee motor to the hip of the robot as seen in Fig. 1.7. This is done to combat one of the largest downsides of a serial configuration which is the large amount of moving mass. This move adds mechanical complexity but can be advantageous if implemented correctly.

1.2.2.2 Parallel Configuration

The parallel configuration features actuators and linkages that form a closed loop kinematic chain. This can be done with a variety of linkage types such as four bar and five bar linkages. This addition of these linkages allows the system to move the motors to the top of the leg, reducing the amount of moving mass and adding stiffness, but these linkages add mechanical complexity to the system [20].

ATRIAS is a robot that implements a parallel leg configuration with both motors located

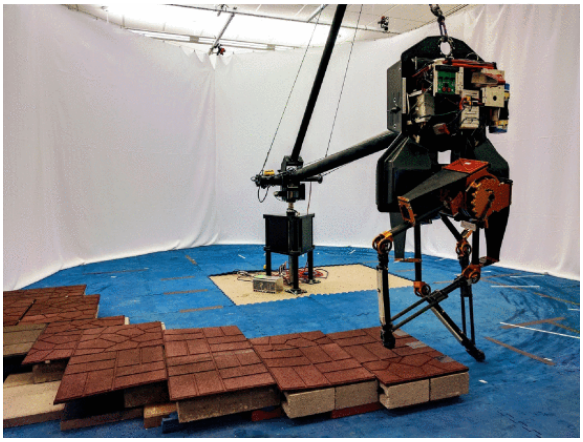

Figure 1.8: ATRIAS bipedal robot[6].

at the hip an connected to a 4 bar linkage as seen in Fig. 1.8[6]. ATRIAS's parallel configuration have proved extremely reliable and shown to accurately reflect SLIP model dynamics.

1.3 Quick State of the Art Review of Leg Architectures

Another consideration when designing for legged robotic systems is the system architecture that the leg will use. This decision governs how the legged system will move as an integrated system and can be split between two categories: sprawling and mammal type systems[21]. A diagram showing each of these architectures can be found in Fig. 1.9.

Sprawling leg architectures take design inspiration from insects who use wide stances to gain additional stability. A sprawling architecture is defined by the first leg link protruding horizontally from the main body. This leg architecture also allows for the center of mass to be lowered closer to the ground further increasing system stability. While TITAN-XIII can be used as an example of a serial leg configuration, it is also an example of a sprawling type architecture as can be seen by its horizontal first leg link in Fig. 1.7.

Mammal type architectures take their design inspiration from various mammals including dogs and humans. This architecture features the first link protruding in a vertical direction such as a human femur. This architecture is not as stable as the sprawling type, but the vertical links allow for reduced power consumption while standing and the lack of horizontal links allows it to pass through much more narrow spaces.

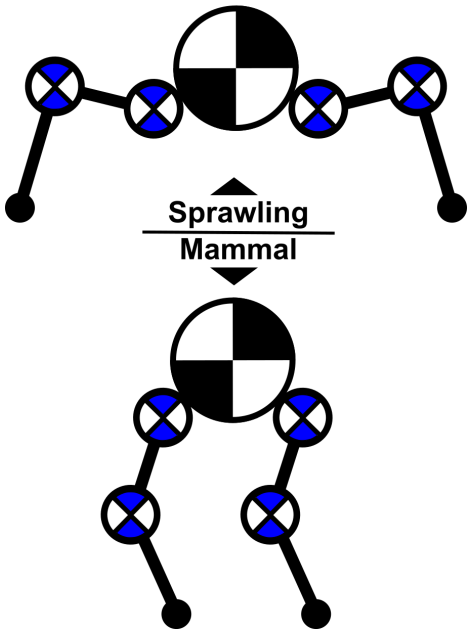

Figure 1.9: Sprawling and mammal type leg architectures.

1.4 Project Goals

Using the principles from the plethora of legged robotic systems, the Harpy robotic system was created with the ability to navigate rough and challenging terrain in mind[22]. However, the mechanical design of the leg does not implement passive elements and mechanical linkages to accomplish tasks in such a terrain to the best of its ability. Additionally, with Harpy's defining feature being flight using thrusters, the leg does not implement any ability to dissipate the energy from large falls that the robot may encounter when performing aerial maneuvers. With these goals in mind, a new leg design was developed with the following objectives in mind.

1. **Agility:** The leg should be able to operate with a wide variety of gaits and should be able to complete these gaits quickly and in a variety of body postures. Additionally, the leg should be able to perform high jumps.

2. **Fall Dissipation:** The leg should be able to dissipate the energy from a high energy fall without sacrificing performance during standard movement.

3. **Robustness:** The leg should implement passive elements and kinematic structures to improve platform robustness in rough and unknown terrain.

Chapter 2

Design Overview

This chapter will first discuss the current Harpy design including its body design, leg design, and actuator design. Next, it will discuss the high level design decisions that were implemented in the binary passive element leg design developed for the Harpy platform. Following the robotic leg design framework, the reduced order model for the system will be covered first. Next, the kinematic design of the leg will be discussed and finally the actuator design will be discussed in brief.

2.1 Overview of Current Harpy Design

Harpy is bipedal, multimodal robotic platform designed by Northeastern's Silicon Synapse Lab[9] in conjunction with other multimodal robotic platforms such as Husky[23][24] and M4[25]. As seen in the annotated diagram of Harpy found in Fig. 2.1, Harpy features two electric ducted fans for performing aerial locomotion and two custom legs for ground locomotion based on the robot LEONARDO[26]. Harpy has been used to perform a variety of successful experiments in multimodal locomotion such as reduced order model control[**?**], feedback control [27], and thruster assisted locomotion[28][29].

Harpy can be broken into two sections: the upper body and the lower body. The upper body utilizes two carbon fiber tubes to secure the actuators that control the angle of the EDFs. The EDFs are actuated to allow the system to perform thrust vectoring opening up a wide variety of movement options [30]. Carbon fiber was used as it will ensure minimal deflection due to the high impulse forces generated by the EDFs while keeping assembly weights low. The EDF support assembly is then mounted onto a back plate that secures all motor controllers required to run Harpy.

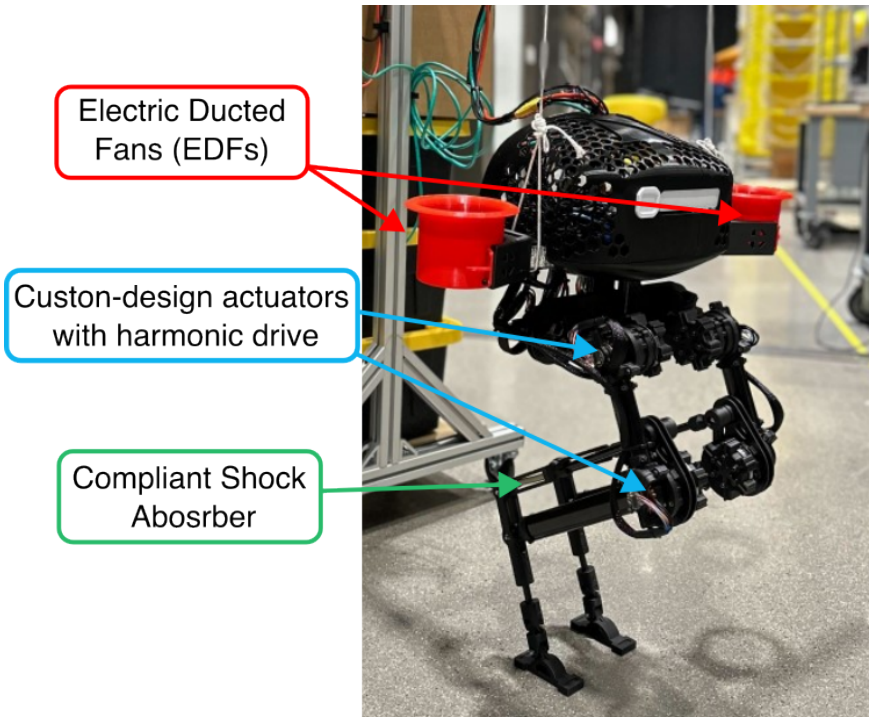

Figure 2.1: Current Harpy platform[7].

For aerial propulsion, EDFs were chosen for their small size to thrust ratio and protected blade structure. The specifications for the selected EDF can be found in Table 2.1.

2.1.1 Current Harpy Leg Design

The lower body consists of two custom designed legs built to be energy dense, lightweight, and robust. The actuators for the leg are arranged in a serial kinematic configuration. To keep the leg lightweight, a pantograph was used as it has high mechanical advantage and efficient use of actuator torques. The use of a pantograph also prevents a singular configuration and inversion of the knee. For the limbs of the leg, a carbon fiber tube with a ovular cross section was used. Ovular tubes were used as the majority of the stress the limbs experience is in the sagittal plane. Using a circular tube cross section would not optimize the tube for the primary force vectors it experiences and thus the leg would require a larger, heavier tube to achieve the same stiffness. By using an ovular cross section, mass is reduced without compromising leg stiffness. The leg can be broken into two sub assemblies: the pelvis assembly and the knee joint. The pelvis assembly connects the upper body to the leg and consists of two actuators. These two actuators make up the hip of the leg and allow

Figure 2.2: Schuebeler DS-38 AXI HDS [8]

Parameter(s)	Value
Max. Thrust	53 N
Max. Exhaust speed	108.3 m/s
Duct weight	100 g
Motor weight	300 g
Duct diameter	80 mm
Duct length	60 mm

Table 2.1: Schuebeler DS-38 AXI HDS EDF with HET 700-68-1400 motor specifications. [31]

the leg to move in both the frontal and sagittal plane. The final actuator for the leg is called the knee actuator. This actuator is used to actuate the pantograph and can dynamically change the length of the leg. One key feature of the pantograph in Harpy's leg is a compliant element. This compliant element, referred to as the shock absorber assembly, decouples the leg end from the knee actuator. This is done to reduce the torque shocks that the actuator experiences during fall impacts. It features a spring that allows the length of the top bar of the pantograph to change, allowing the leg end to be moved without changing the position of the knee actuator. The current Harpy leg can be found in Fig. 2.3.

2.1.2 Current Harpy Actuator Design

Harpy's current actuator features a BLDC motor, harmonic drive, and encoder. A BLDC motor was selected for its high torque density and lightweight construction. BLDC motors have proven extremely power dense in many applications such as drones and thus are suitable for robotic applications. However, it is important to keep the motor well below its rated power output as this power output assumes active cooling being provided by drone propellers. As the Harpy actuator does not feature active cooling, running the BLDC motor at its rated maximum continuous power may cause overheating and premature failure. The specifications for the BLDC motor selected can be found in Table 2.4. When considering the torque requirements for Harpy's leg, it was determined that direct drive would not be suitable and thus a transmission would be required. A harmonic drive was chosen to serve as the actuator transmission for its lightweight construction, high backdrive-

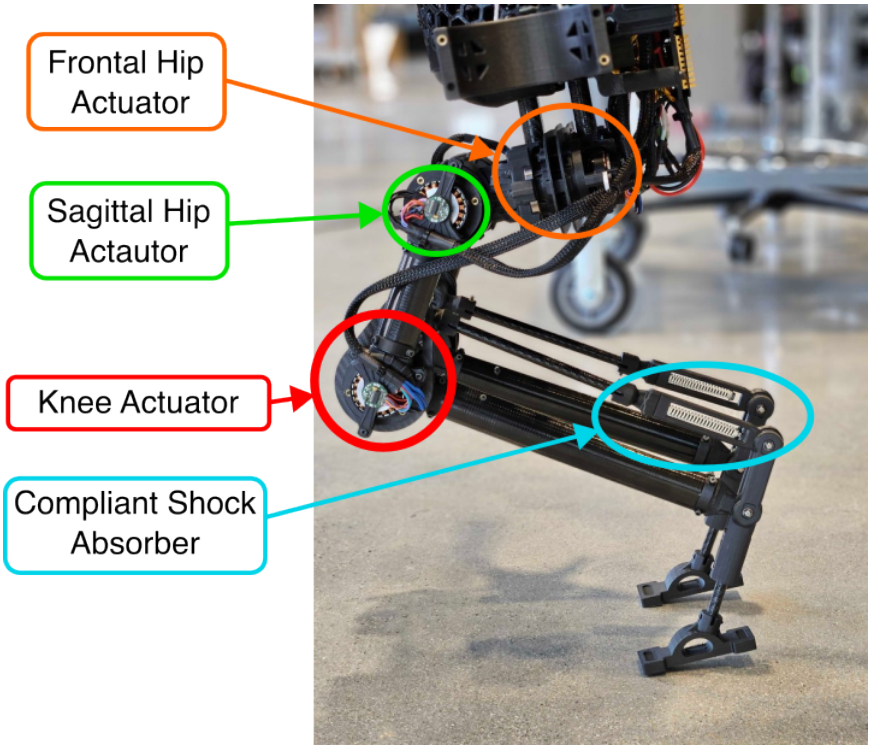

Figure 2.3: Current Harpy leg.

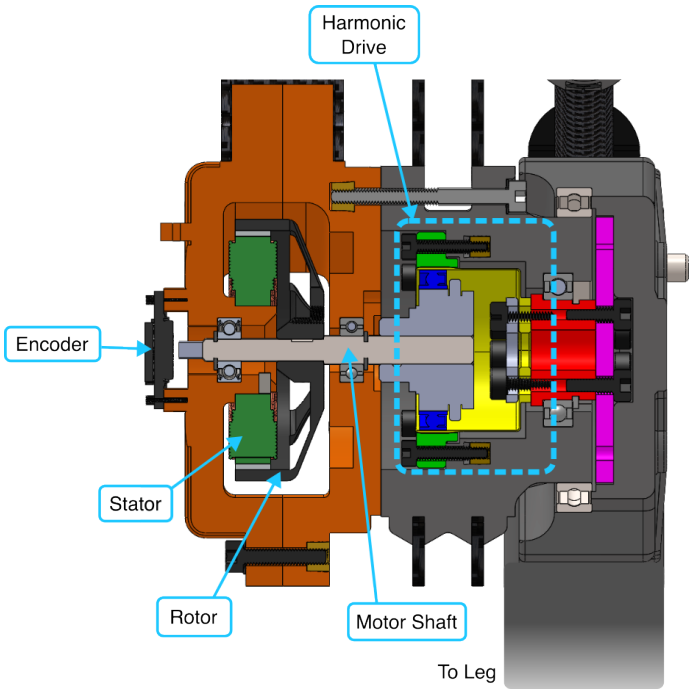

Figure 2.4: Current Harpy actuator.

ability and precision output due to it featuring an very small amount of backlash. The specifications of the chosen harmonic drive can be found in Table 2.2. Finally, a hall effect based encoder is used for relative position sensing. The specifications for the selected encoder can be found in Table 2.3. A cross section of the current Harpy actuator can be found in Fig. 2.4.

2.2 Overview of the Binary Passive Element Leg Design

This section will discuss the reduced order model, kinematic configuration, and briefly discuss the actuator design for the binary passive element leg.

2.2.1 Reduced Order Model

The reduced order model for the BPE leg consists of two sets of spring and damper sets as seen in Fig. 2.7. Both spring and damper sets are placed in parallel with the actuator however only one set is always connected to the leg end. This set is referred to as the attached spring and damper. The second set is left slack and only influences the model dynamics once the leg end has moved past a designed region of the task space. With each of these elements able to have their own

Parameter	Value
Gear ratio	30
Peak torque limit	8.5 Nm
Backdriving torque	1.3 Nm
Max. input speed	8500 rpm
Backlash	2.3 $\times 10^{-5}$ rad
Weight	50 g
Overall length	25.8 mm
Circular spline diameter	40.0 mm

Table 2.2: Harmonic Drive CSF-11-30-2A-R specifications.[32]

Figure 2.5: RMB20 encoder module [8]

Parameter	Value
V	5V
Max. Current	35 mA
Accuracy	0.5 deg
Resolution	8129

Table 2.3: RMB 20 specifications[33].

Figure 2.6: T-motor Antigravity 4006 [9]

Parameter	Value
KV	380
Max. Continuous Power	380 W
Max. Continuous Torque	0.447 Nm
Continuous Current Limit	14 A
Weight	68 g
Rotor Diameter	44.35 mm

Table 2.4: T-motor Antigravity 4006 specifications[34].

element constants, the system can be designed to exhibit very different behavior inside and outside of the slack effected region. The two stages of effective damping and spring constant values is what is referred to in the name binary passive element leg.

As each of these elements have associated constant values that are able to be tuned during design, it is critical to identify what purpose each element serves so that analysis can be used to effectively design element constants. First, the attached springs primary purpose is to reduce the required actuator torques allowing for a wider variety of task space gaits. This spring has secondary purpose of increasing fall and jump heights by storing energy when the leg is in a compressed configuration. Second, the attached dampers purpose is to increase leg robustness as shown by the research of Heim et al. It also serves a secondary purpose of dissipating energy during falling motions, thus increasing maximum fall heights. However, the attached damper is designed to be quite weak meaning that the damper will not have a significant effect on the maximum fall height of the system but also meaning that the system will not suffer an unsustainable CoT increase. Finally, the primary purpose of both the slacked spring and damper is to absorb energy during high falls. In the hardware implementation of the BPE leg, the slacked spring and damper are combined into a single shock absorber unit. This shock absorber is used to most effectively absorb high falls that would normally overload the actuators and cause the leg to either overshoot angle limits or slam into actuator hard-stops, both of which have a large potential to cause damage to the leg or the rest of the robotic system.

2.2.2 Kinematic Design

The kinematic configuration selected for the BPE leg is a five bar parallel configuration as seen in Fig. 2.8 along with its associated parameters.

A parallel kinematic configuration was chosen for its system benefits and geometric constraints. The primary system benefit that led to the choice of a parallel kinematic configuration was the reduced moving mass. This allows the system to react quickly to rapidly changing control inputs in difficult terrain. Additionally, the added stiffness of a parallel kinematic configuration will assist in high acceleration maneuvers such as the impact from a fall.

A parallel kinematic configuration was also chosen for geometric reasons. It is important that the system is able to make use of the maximum amount of actuator travel and accommodate a shock absorber. By using a configuration that requires a large angle delta from the fully extended configuration to the fully compressed configuration, a maximized amount of work can be done by

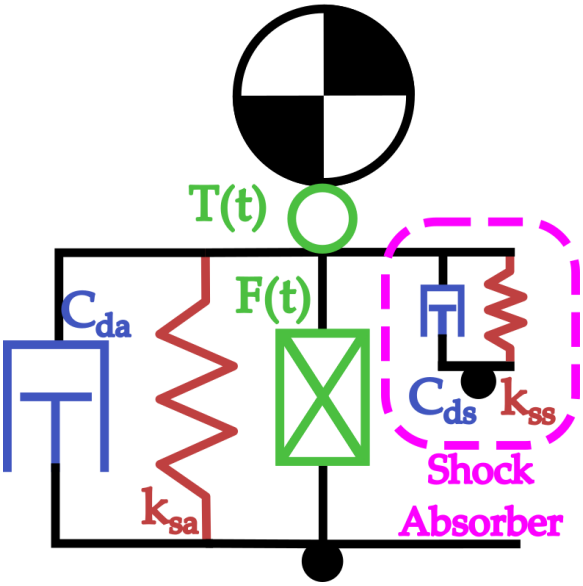

Figure 2.7: BPE reduced order model.

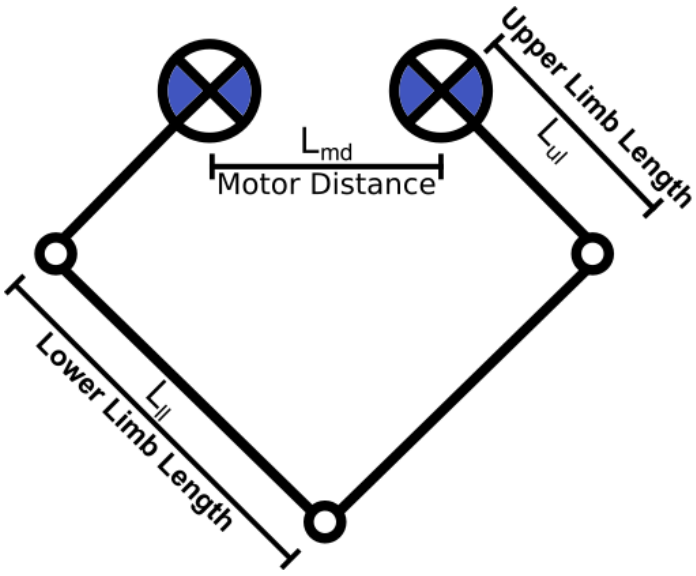

Figure 2.8: BPE kinematic configuration.

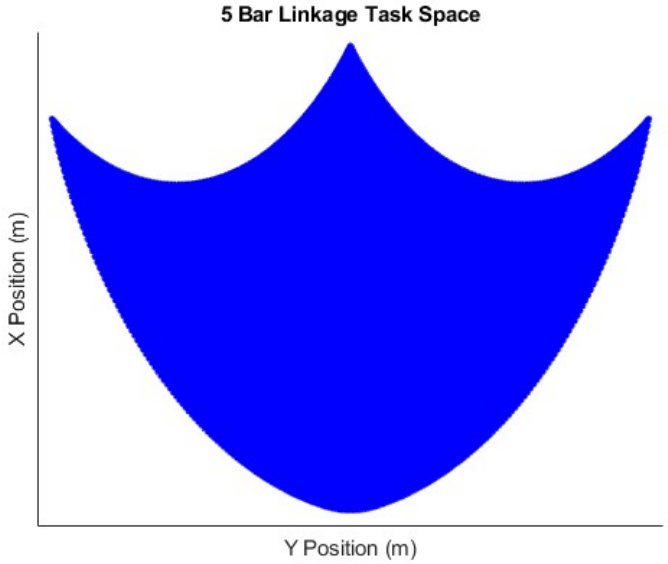

Figure 2.9: Five bar linkage example task space.

the actuator. This allows for more energy to be output during jumping maneuvers and absorbed during falling maneuvers. The use of a shock absorber in the hardware system presents unique challenges for the BPE leg. The first of these challenges is mounting a shock absorber. The shock absorber is mounted between the two actuators and allowed to pivot around a point centered on the fifth link. This was done to assist in the next challenge of implementing a shock absorber: how to engage the shock absorber during high fall maneuvers. As is shown in the BPE reduced order model, the shock absorber only applies force to the leg end in the case that the leg end enters the slack impacted area of the task space. The shape of the five bar linkage task space can be utilized to allows for large end effector positional error during falling maneuvers while ensuring proper shock engagement. Fig. 2.9 shows the task space of a five bar linkage kinematic configuration given a maximum actuator angle and link lengths. As can be seen, the task space funnels the end effector position to the center as long as the leg can maintain a position within the two local minima of the two curves that define the top of the task space. As the shock is placed in the center of the actuators, this means that the foot will be funnelled into the shock absorber when the actuators are overpowered by the impact of a large fall.

2.2.3 Actuator Design

As actuator design was not a primary focus of the research conducted for this thesis, many design decisions were borrowed from the previous actuators designed for the Silicon Synapse Lab. However, the actuator did receive some updates to implement the updated reduced order model. These updated will be fully discussed in Chapter 4 with the full CAD discussion.

Chapter 3

Variable Selection

As for any design challenge, proper selection of values for design parameters is critical to the function of the system. In this chapter the selection theory for all major leg parameters will be discussed. In addition, the discussed analysis will be performed for a Harpy BPE leg implementation designed around an off the shelf shock absorber.

3.1 Shock Absorber Selection

3.1.1 Theory

Design for the BPE leg begins with shock absorber selection. A shock absorber can be characterized by two variables, maximum impact velocity and energy absorbed per cycle. In theory, these two variables can be designed to achieve any fall height desired. However designing these variables without considering other system components can lead to a unsustainable deceleration rate. If we consider the ideal shock absorber force output curve seen in Fig. 3.1 and approximate that all system energy will be absorbed by the shock absorber, a shock absorber could be designed to dissipate all system kinetic energy for a desired fall height at a given deceleration rate if the system mass is known. This calculation would result in stroke length and a shock absorber could be designed for the desired impact velocity, dissipation energy, and stroke length.

3.1.2 Analysis for Harpy Leg

As designing a custom shock absorber was out of the scope of this thesis, an off the shelf shock absorber was selected to allow for maximum impact velocity given a 6kg approximate robot

Dimension	Length (mm)
Body Length	162
Stroke Length	50

Table 3.1: Enidine ECO 220-1 Geometry

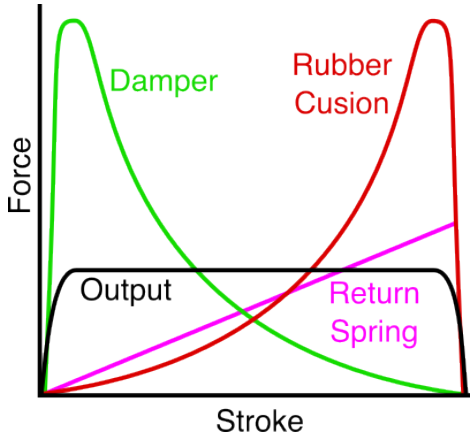

Figure 3.1: Ideal shock absorber force vs stroke position curve[10].

mass. The ENIDINE ECO 220-1 shock absorber was selected allowing for an approximately 4.5 m/s impact as defined in Table 3.2. This selection allows us to find the geometric parameters of the shock absorber as found in Table 3.1

3.2 Limb Length Selection

3.2.1 Theory

With the shock dimensions set, the limb lengths can be determined using the methodology described in this section. This first begins by picking the following variables:

1. Motor Distance: Distance between the two actuators as shown in Fig. 2.8
2. Standard Gait Width: The width of the stance phase of the desired gait
3. Standard Gait Height: The distance from the actuator height to the stance foot height
4. Actuator Maximum Angle: The maximum angle the actuator can rotate to before hitting a hard stop

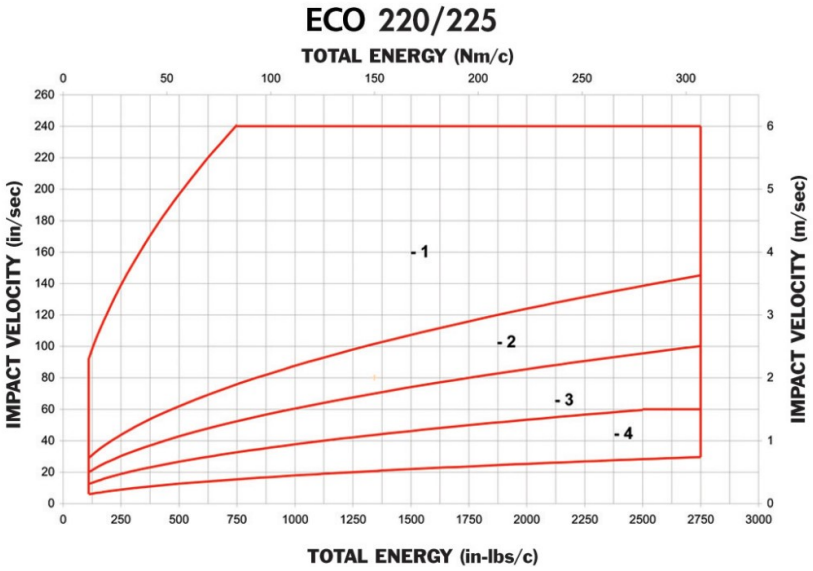

Figure 3.2: ENIDINE ECO 220 impact velocity vs energy per cycle curve[11].

5. Maximum Knee Angle: The angle of the knee at the beginning and end of the stance phase

With these parameters chosen, two geometric configurations can be solved to determine the required limb lengths assuming that the lengths of the two upper limbs and the two lower limbs are equal. The first of these configurations can be seen in Fig. 3.3a. This configuration ensures that when the leg takes a long fall, the full actuator travel is utilized before the shock absorber hits the end stop and that the shock absorber hits the end of its stoke as the upper limbs hit the maximum actuator angle. The second of these configurations can be found in Fig. 3.3b. This configuration ensures that the leg is able to reach a designed maximum gait path with the shortest limb lengths.

3.2.2 Analysis for Harpy Leg

Using the theory outlined in the section above, the limb lengths for the BPE leg Harpy implementation were determined. The values used for this implementation can be found in Table 3.2. Solving for the limb lengths gives the values found in the second column of Table 3.3. These lengths were then rounded to the values found in the third column.

With the limb lengths now chosen, the task space for the leg can be simulated and the gait design can be visualised as seen in Fig. 2.9. Using this visualisation, the shock constraint can also be seen. In Fig. 3.4, the top of the task space can be seen to be approximately 160mm below the actuator center line, which is equivalent to the body length of the shock absorber.

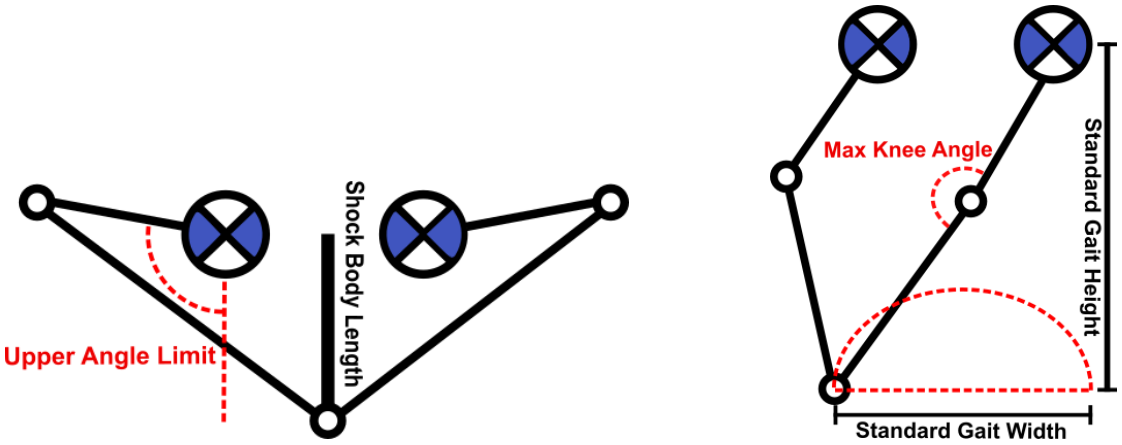

(a) Fully compressed leg state.

(b) Fully extended leg state.

Figure 3.3: Geometric configurations solved to determine limb lengths.

Dimension	Value	Unit
Motor Distance	130	mm
Standard Gait Width	500	mm
Standard Gait Height	500	mm
Actuator Maximum Angle	110	deg

Table 3.2: Harpy leg design parameters.

3.3 Spring Constant Selection

3.3.1 Theory

As one important function of robotic legs is the ability to walk and thus it is important that a single leg is able to support the mass of the robot. Specifically, the leg must be able to act as the stance leg in a wide variety of gaits and thus must be able to support the whole robot weight in a majority of the total task space. One issue of the five bar kinematic configuration is that as the leg

Dimension	Calculated Length (mm)	Selected Length (mm)
Upper Limb Length	225.6	225
Lower Limb Length	365.9	366

Table 3.3: Harpy leg limb lengths.

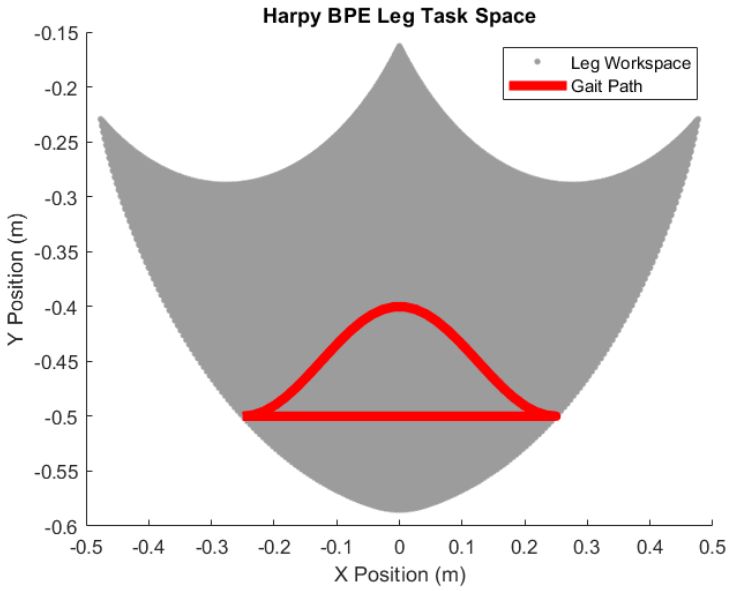

Figure 3.4: Model BPE leg task space.

compresses, the torque required to support a vertical force at the leg end increases due to the larger moment arm being applied to the actuator. This problem can be partially alleviated by including torsional spring elements in the knee of each of the leg segments. The areas of the task space that can be used for walking can be solved for using static analysis performed in MATLAB. If the mass of the robot is known, a vertical force can be applied to the foot and motor torques can be solved in any given leg configuration. The force body diagram for this system can be seen in Fig. 3.5.

After solving for the motor torques across the configuration space, the walkable and unwalkable area can be plotted. If this area is less than desired, a torsional spring can be added to the static analysis and the walkable areas can be recalculated. As the spring stiffness increases, more area of the task space will become walkable at the cost of an increase to the energy required to operate in a standard gait cycle.

To estimate how much energy the spring is costing the system, an analysis of the energy required to complete a single gait cycle was performed. This analysis was performed in Simulink for the desired gait path. By recording the actuator torques, the energy consumption for different spring rates can be compared to the no spring system. This was done by integrating the square of the torques over a single gait cycle for different spring rates and dividing by the integrated torque of the no spring system as is done in the equations below.

$$P_n = i^2 R$$

$$\tau_n = K_t i$$

$$P_n = \frac{R}{K_t^2}\tau_n^2$$

$$\int_0^t P_n = \frac{R}{k_t^2}\int_0^t \tau_n^2$$

$$E_n = \frac{R}{k_t^2}\int_0^t \tau_n^2$$

$$E_n \,\%\, Change = \frac{\int_0^t \tau_n^2}{\int_0^t \tau_0^2}$$

where

- τ_n is the recorded torque data for a leg with a spring constant of n.
- K_t is the motor torque constant
- i is the motor current
- R is the motor resistance
- P_n is the power being consumed by the motor for a spring constant of n
- E_n is the energy consumed for a single gait cycle for a spring constant of n

By balancing the benefit of additional walkable area to the cost of additional energy requirements, a spring constant for the knee can be chosen.

3.3.2 Analysis for Harpy Leg

To begin the spring analysis for the Harpy BPE leg, first an estimated robot mass and actuator torque limit must be specified. These values for the Harpy implementation can be found in Table 3.4. With these values the no spring walkable space can be generated using a statics solving package in MATLAB as can be found in Fig. 3.6a.

This figure shows that the robot would be severely restricted in taking steps at any amount of crouching position or stepping up a stair of most heights. This validates the need for a knee spring for the system but more analysis must be done to determine the strength of this spring. In Fig. 3.6b,

Variable	Value	Unit
Robot Mass	6	kg
Actuator Torque Limit	8.3	Nm

Table 3.4: Harpy leg spring design parameters.

it can be seen that including a knee spring with a spring rate of $0.05\frac{Nm}{deg}$ opens up the walkable task space considerably. Additionally, using Simulink the energy cost of the springs can be compared as seen in Fig. 3.7. For this implementation of the BPE leg, a spring rate of 0.05 Nm/deg was chosen costing the system an additional 6.17% in energy consumption.

3.4 Damping Constant Selection

3.4.1 Theory

With the spring chosen. the final variable to select is the value of the attached damper. This damper will be selected using the analysis from the paper "A little damping goes a long way"[17]. In this paper, the effect of damping on the ability for a system to stay stable after encountering a ground height perturbation was analyzed. The analysis in this paper was performed on a DASLIP model as shown in Fig. 1.1e. This model does not exhibit the same dynamics as the model used for the BPE leg however completing their analysis for the BPE model was determined to be out of the scope of this thesis, thus their findings for the DALSIP model are applied to the BPE model.

In their findings, they determined that damping increases the robustness of a system until it begins to plateau at a relatively small damping value. This value was found to be $k_s\sqrt{\frac{l_0}{g}}$ where

- k_s is the spring constant
- l_0 is the unloaded length of the spring
- g is the acceleration of gravity

Using Simulink, the approximate linear spring constant can be found for a given leg configuration and knee spring constant. Then, using Standard Gait height for l_0, the desired damping constant for the system can be calculated. A desired damping value of three quarters calculated value was chosen to final energy cost of the damper. Simulink can then be used to find the rotary damper constant that approximates the desired linear damping constant.

3.4.2 Analysis for Harpy Leg

To begin the damper analysis for the Harpy leg, the approximate linear spring constant must be found. This was completed in Simulink and analyzed in MATLAB. The model that was used to perform the analysis for the spring and damper can be found in Fig. 5.7. The results for the spring analysis found in Fig. 3.8, shows the approximate spring constant to be 108.8 N/m. Using the standard gait height found in Table 3.2, the desired equivalent linear damping value is calculated to be 18.4 Ns/m.

Again, Simulink and MATLAB are used to determine the rotary damper constant needed to approximate this linear damping constant. This was done by first recording the force needed to raise the leg end at $0.1\frac{m}{s}$ with a damping value of zero. Then the same data was recorded for a damping constant of $425\frac{oz-in\ s}{rad}$. By subtracting the undamped data from the damped data, the additional force required to raise the leg due to the damper was isolated. This force data was then approximated into a equivalent linear damping constant. This analysis can be seen in Fig. 3.9. Using this method a equivalent linear damping constant of $17\frac{Ns}{m}$ was calculated. This was determined to be sufficiently close to the calculated damping value that a rotary damping value of $425\frac{oz-in\ s}{rad}$ was used in the hardware implementation.

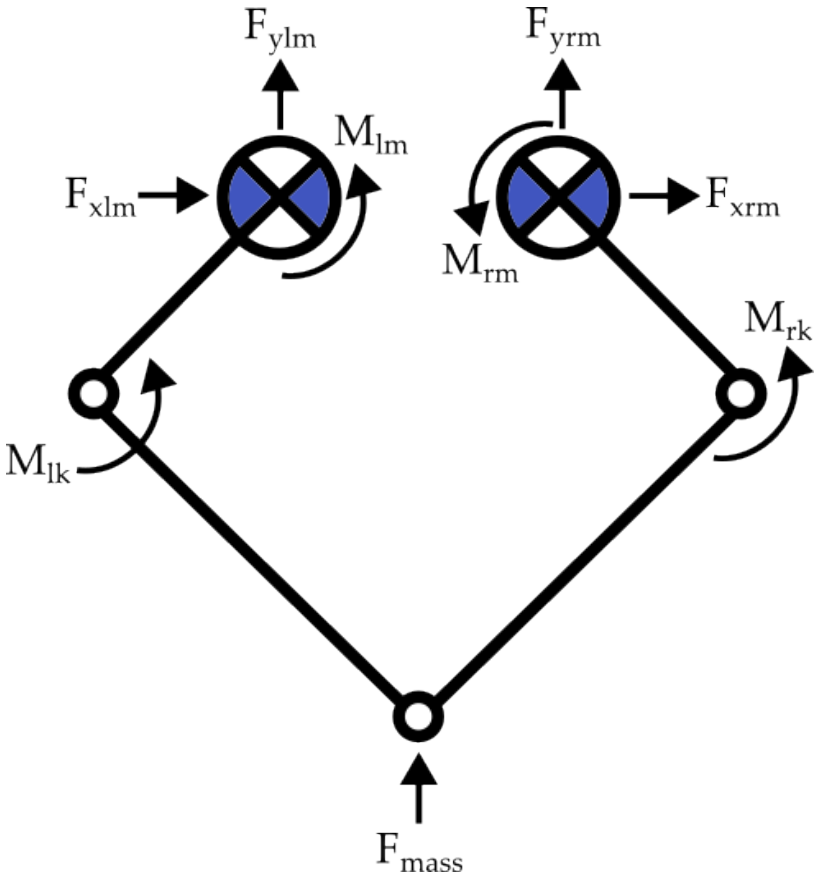

Figure 3.5: 5 Bar Force Body Diagram where F_{xlm}, F_{ylm}, F_{xrm}, F_{yrm}, M_{lm}, M_{rm}, M_{lk}, M_{rk}, F_{mass} are the left motor reaction force in the X, the left motor reaction force in the Y, the right motor reaction force in the X, the right motor reaction for in the Y, the moment applied by the left actuator, the moment applied by the right actuator, the moment applied by the left knee spring, the moment applied by the right knee spring, and the ground reaction force respectively.

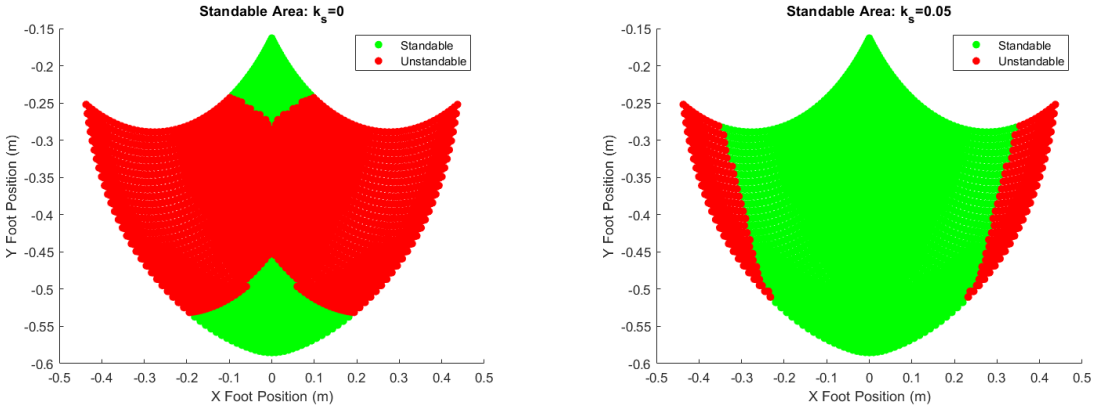

(a) No spring walkable task space.

(b) $0.05\frac{Nm}{deg}$ Spring Walkable Task Space

Figure 3.6: Harpy BPE leg walkable regions of the task space.

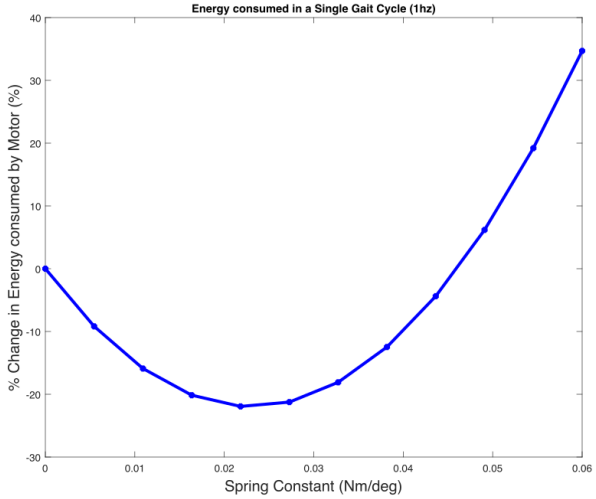

Figure 3.7: Spring energy cost curve.

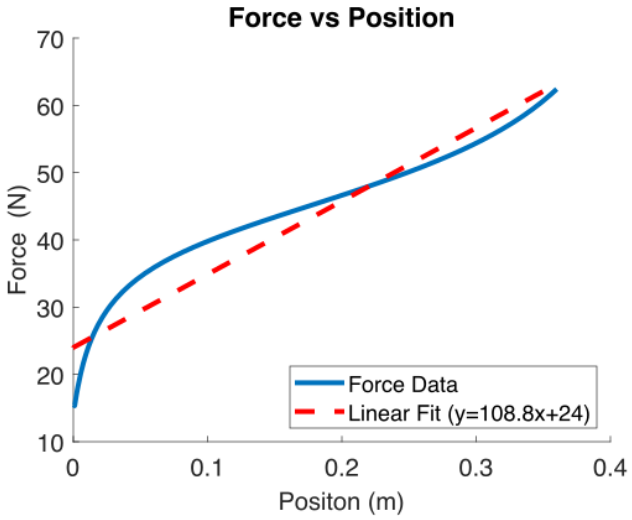

Figure 3.8: Spring constant analysis results from Simulink.

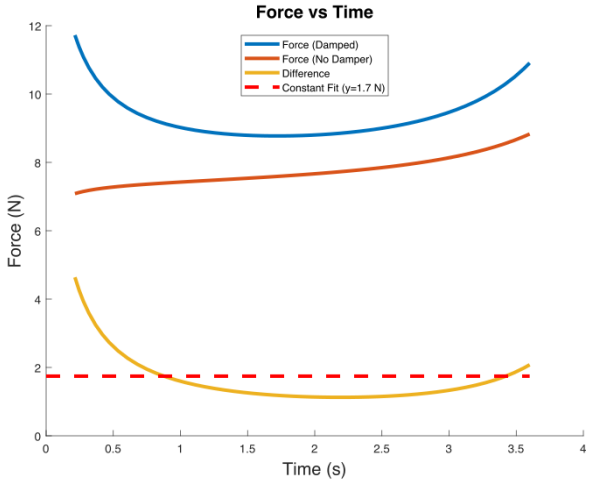

Figure 3.9: Damping constant analysis results from Simulink.

Chapter 4

Hardware Design

With system parameters selected for the Harpy implementation of the BPE leg, the final step in robotic leg design, hardware design, can be performed. This chapter will cover the BPE leg hardware design consisting of four primary subsystems. Those subsystems are the actuator, the knee, the foot, and the shock absorber. The systems are designed to implement the BPE model, kinematic structure, and parameter values specified in the Harpy BPE implementation up until this point. The CAD produced in this chapter can be found in the Silicon Synapse PDM vault at the file location: .\PDM\Silicon Synapse Lab\Harpy\Harpy Leg Redesign.

4.1 Actuator Design

The most complex of the leg subsystems is the actuator. The actuator consists of four primary components. Those are the motor, the sensing element, the gearbox, and the attached damper. For these major components, the hardware solutions can be found in Table 4.1.

A custom enclosure and supporting hardware were implemented to produce a finished

Feature	**Part**	**Part Number**
Motor	Brushless DC Motor	T-motor Antigravity 4006
Gearbox	50:1 Harmonic Drive	CSF-11-50-2A-R
Sensing	Hall Effect Encoder	RMB20
Damper	425 oz-in Dual Direction Damper	6597K117

Table 4.1: BPE actuator components.

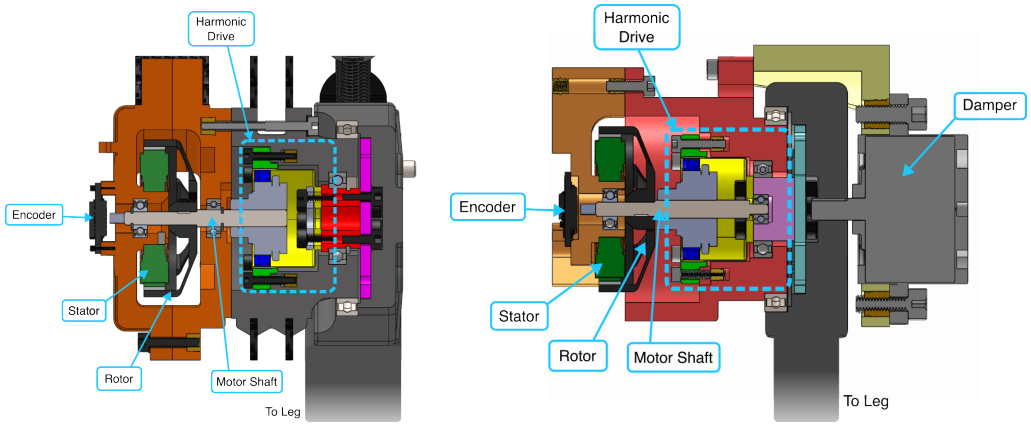

(a) Current Harpy actuator assembly. (b) BPE leg actuator assembly.

Figure 4.1: Current Harpy actuator and new BPE leg actuator comparison.

actuator that additionally featured surface mounting and connection point for the upper limb. The finished actuator design can be found in Fig. 4.1b.

To design the actuator, many design decisions were carried over from the current actuator implemented on the Harpy platform, however many changes were made to effectively implement the new passive elements. The changes made to the actuator are

1. **M**ounting: Mounting was shifted from mounting to a link end to mounting to a surface
2. **D**amping: A damping element was added to the actuator output
3. **B**earing placement: Internal transmission bearing was shifted

The following design decisions were carried over from the previous design

1. **M**otor Selection: The current brushless DC Motor currently in use on Harpy
2. **G**earbox Selection: The current Harmonic drive currently in use on Harpy
3. **T**ransmission components: The shaft and bearing sizing

In Fig. 4.1, the cross sections of the original actuator design and the updated actuator design can be seen. The changed made to the actuator are significant enough to require a redesign, however the overall design concepts of original actuator has stayed the same.

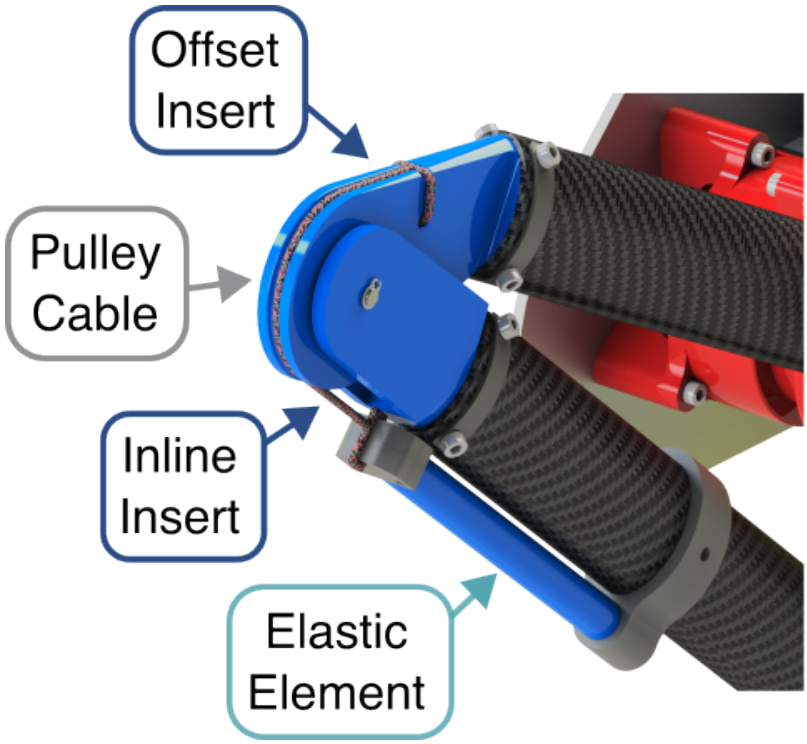

Figure 4.2: BPE knee assembly.

4.2 Knee Design

The knee subsystem needs to implement the spring constant derived in Chapter 3 as well as allow for small angle configurations. To accomplish this, the knee design features an extension spring and pulley system to replicate the designed spring rate of 0.05 Nm/deg. Additionally, it features and offset in the upper limb insert, allowing for a minimum knee angle of 25 degrees, the angle of the knee in the fully compressed configuration. The final knee design can be found in Fig. 4.2.

4.2.1 Knee Spring Design

Initially, torsion springs were investigated to serve as the knee springs, however torsion springs of the appropriate constant were found to be too large to fit within the knee assembly. Therefore, an extension spring in conjunction with a pulley were investigated. By using an extension spring along the length of the lower limb, the footprint of the spring was reduced. To turn the force applied by the spring to a torque applied to the knee, a pulley centered about the knee pivot point

was built into the lower limb insert. A cable of appropriate strength could then be wrapped about the knee and connected to the end of the extension spring.

Initially, off the shelf steel extension springs at the desired spring rate were investigated but also proved too large to fit within the geometry of the knee. In place of a standard steel extension spring, an elastic element was substituted. This elastic is designed to be EPDM cord stock in a 10mm diameter however the Young's Modulus of EPDM cord stock proved to have a very wide range and no suppliers listed a known Young's modulus. This required that the knee be designed to accommodate the possible range of Young's moduli. To accomplish this, the fixed point of the elastic element was designed to be able to be mounted at any point along the length of the lower limb. By allowing a variable elastic element length, the amount of strain the elastic element experiences from the fully extended configuration to the fully compressed configuration can be adjusted. This allows for the amount of force the elastic element produces at its full extension to be tuned to the desired value. With the lower limb insert pulley set at a fixed diameter, the displacement of the elastic element was calculated to be 59.5mm. This results in a strain of 214% with a Young's Modulus of 210 Mpa, the lower bound for EPDM, and a strain of 73% with a Young's Modulus of 614 Mpa, the upper bound for EPDM. Both of these strains are lower than the maximum tensile strain of EPDM which is 250%.

4.3 Foot Design

The foot subsystem has two primary design considerations, the minimum foot angle and the foot-shock interaction. To allow for small angle configurations, the foot design features an offset insert similar to the knee insert. For the foot-shock interaction, a curved extrusion on its rear of the foot was made to interface with the end of the shock absorber. The final foot design can be found in Fig. 4.3.

4.3.1 Foot-Shock Interaction

The primary objective of the foot-shock interaction is ensure proper contact and alignment of the shock absorber with the foot. To accomplish this, two design considerations were made. The underlying principle of this interaction can be derived from the BPE leg task space. As seen in Fig. 4.4, the extended length of the shock absorber extends slightly into the task space of the leg. Knowing the length of the extended shock absorber, the width of the task space at this height can be

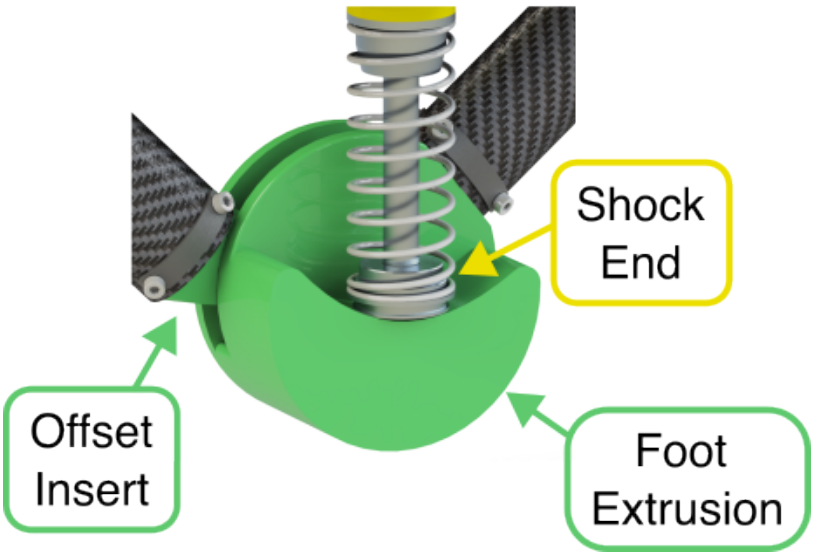

Figure 4.3: BPE foot assembly.

determined. For the Harpy BPE leg, this width was found to be approximately 75mm. As the leg may not have full control of the leg end position when impacting the ground, it is critical that the foot can not miss the foot curved extrusion. Thus the foot was designed to have an 80mm diameter necessitating that the foot impact the shock absorber end even if the foot is collapsing toward to the shock absorber along the edge of the task space.

4.4 Shock Absorber Design

As was explained above, the shock absorber is able to impact the foot at the edge of the task space and to ensure proper contact the foot features a curved extrusion to center the shock end. To allow for the centering of the shock absorber to occur, the shock absorber is mounted using only a single bolt. This allows the shock absorber to rotate and align itself with the center of the foot. However, this contact is only guaranteed assuming that the shock absorber is currently centered in the task space. To ensure that the shock absorber remain centered in the task space, a strong extension spring is placed at the top of the shock mount, pulling the shock to a vertical, centered position. Additionally, no bearings were used in the mounting location of the shock mount as the friction produced between the bolt surface and the mounting surface can be used to decrease oscillations in the actuator angle that may be induced under standard walking conditions. The final shock absorber mounting solution can be found in Fig. 4.5.

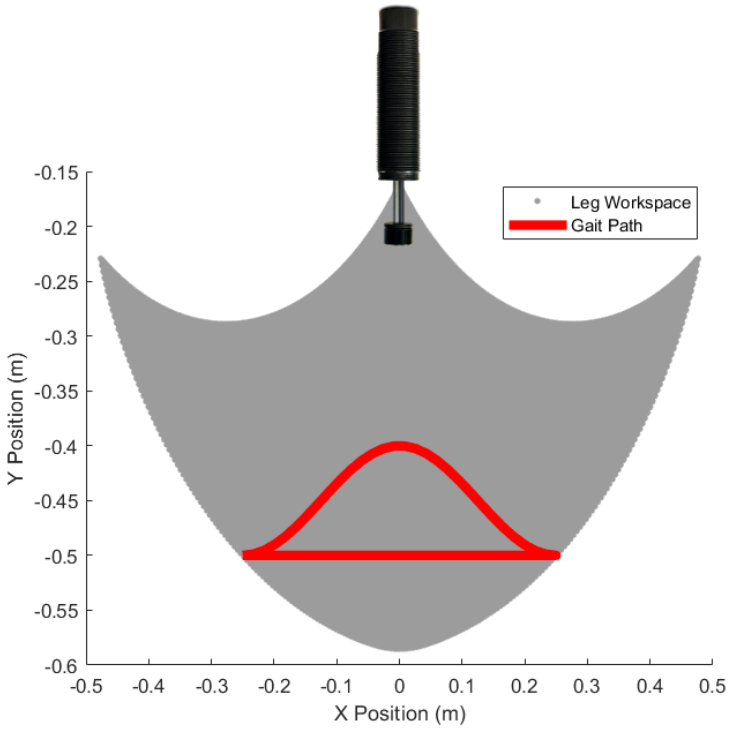

Figure 4.4: Shock absorber relative to task space.

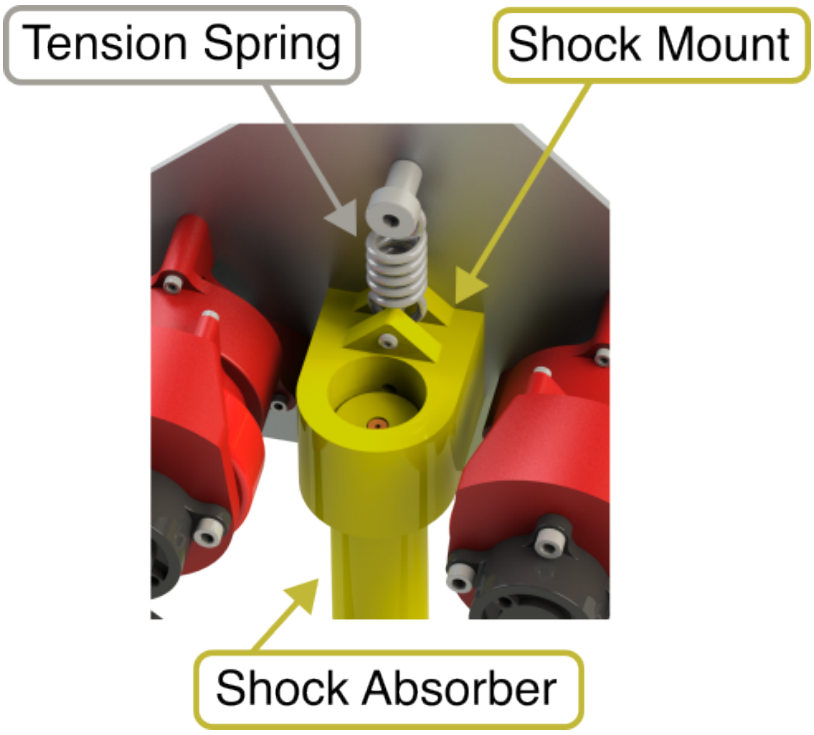

Figure 4.5: Shock absorber mount assembly.

4.5 Complete System

With all subsystems of the leg designed, the leg can be assembled and final system renders can be generated. These renders can be found in Fig. 4.6.

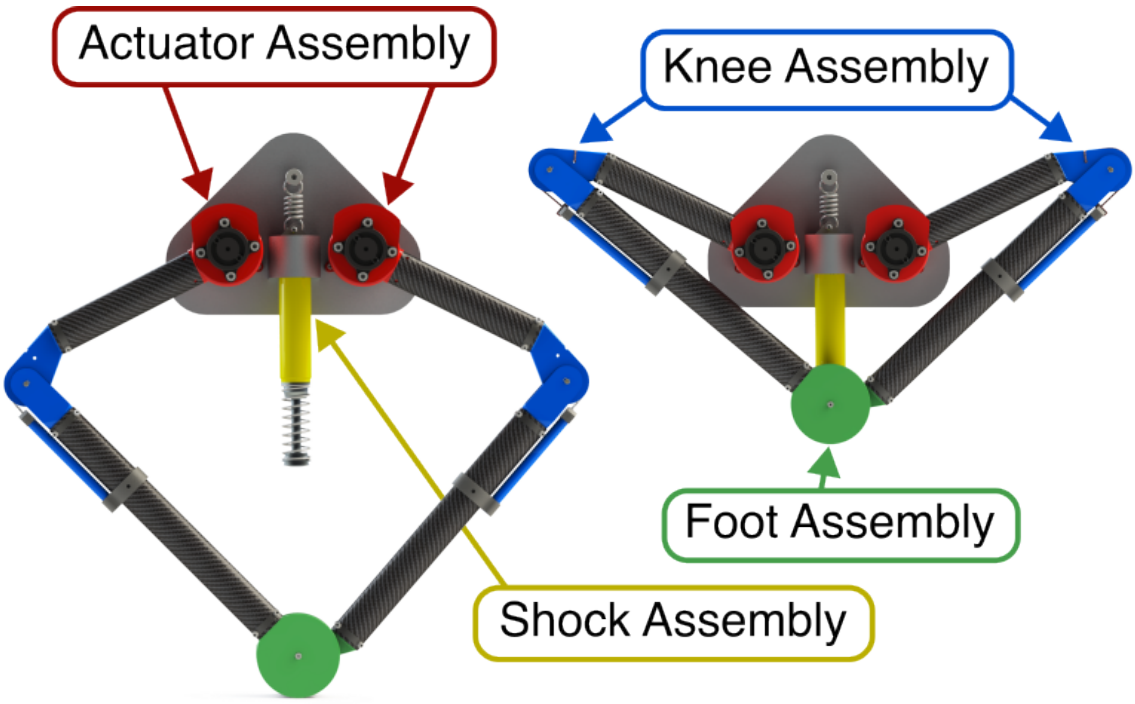

Figure 4.6: Final leg render in both extended and compressed configurations.

Chapter 5

Simscape Models

The test the validity of the design, two models were built in Simscape to test the two primary function of the BPE leg design, falling and jumping. These Simscape models implemented the design parameters along with the CAD designed in Chapter 4. This chapter will discuss the construction of these models along with the relevant design decisions that were implemented. This chapter will also discuss the models used for solving for the attached damper value and the spring cost. The code and models referenced in this chapter can be found in the Silicon Synapse Lab Github at the file location: .\harpy-modelling\BPE Leg Modelling and Analysis Tools

5.1 BPE Model Implementation

As both models used to test the leg implement the BPE leg CAD and design parameters, they feature a lot of shared components. Those components include the actuator model, the leg model, and the shock absorber model. These three components for the jumping model can be seen highlighted in Fig. 5.1. The implementation of the actuator and shock components are not the same across simulators thus its implementation will be explored in future sections. However, the leg implementation is equivalent in all simulators. The implementation of the left leg can be seen in its full in Fig. 5.2.

Both leg models feature two rigid bodies for the upper and lower limbs and a revolute joint to act as the knee. The knee joint implements two key values; equilibrium point and spring stiffness. For the knee spring implementation, the equilibrium value is set for each knee such that the knee spring is in equilibrium when the lower and upper limbs are co-linear. The spring stiffness determined in chapter 4 is simply set as the joint spring stiffness. In addition, the left leg features

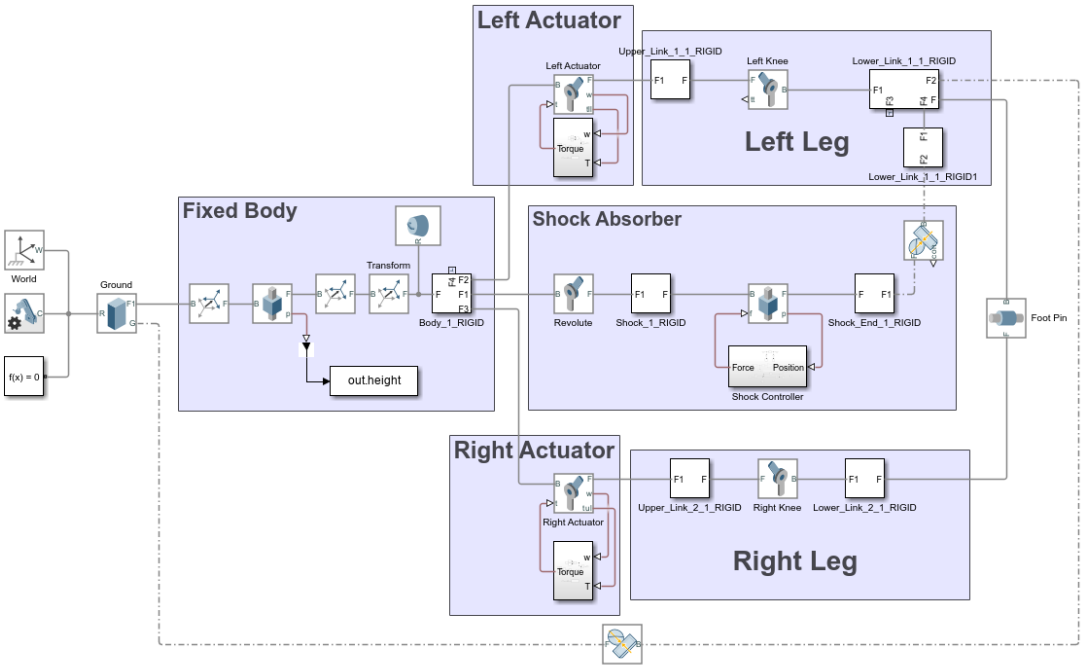

Figure 5.1: Simscape model overview.

an added rigid body for the shock interface extrusion. This was added as an additional part to the left lower limb due to the geometry export properties of Simscape contact. To do collisions, Simscape compares the convex hull of the rigid bodies in collision. Due to the lower limb being a large combination of CAD components, the convex hull was not accurate and this led to improper collisions between the shock end and the foot. To reduce this error, the shock interface extrusion was exported from CAD as a single body and added as a separate component into the model. The contact modelling was then performed between only this small extrusion and the shock end. This greatly reduced the error in the model when simulating shock-foot contact.

5.2 Jumping Model

The first of the Simscape models produced was the jumping model. The purpose of this model was to analyze the final jump height of the system after implementing the attached passive elements. The model features two stages. The first of these stages is when the leg crouches into its most compressed position. The model then sits in that position until it jumps into the air, reaching its maximum jump height.

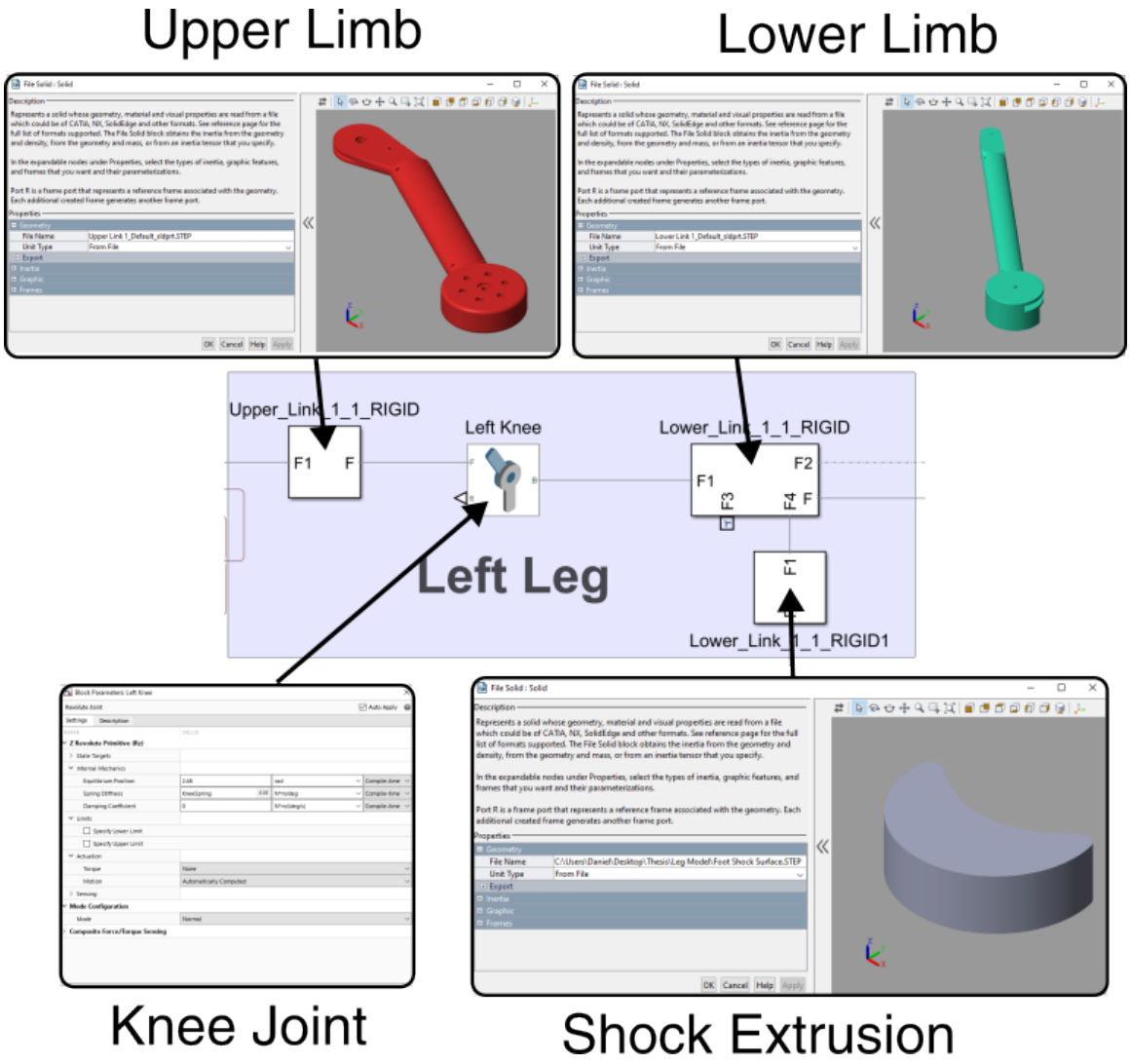

Figure 5.2: Left leg model with added shock extrusion body.

This two stage movement by the actuators is accomplished using simple switches and torque signals. The actuator model for the jump simulator can be found in Fig. 5.3. Inside of the revolute joint that defines the motion of the actuator joint, both a minimum and maximum actuator angle has been set based on the leg design parameters. Inside of the actuator controller block there are two distinct paths in which torque is generated. The first of these can be seen on the top and this is the torque that is generated by the motor. The bottom path represents the torque generated by the damper. This damper model is utilized in both the jumping and falling simulator. To achieve the two stage movement seen in the simulation, a torque is applied to move the actuator to the upper angle limit. After letting the system settle in this position, the torque is reversed and the leg jumps into the air.

To generate the torque from the damper, a piece-wise function was assumed where the damper generates torque linearly proportional to the input rotational velocity. However, after the rotational velocity exceeds a maximum value, the damper continues to generate constant torque value equivalent to the torque being output at the maximum rotational velocity. For both models, the maximum rotational velocity was set to 50 rpm and the maximum damping torque was set to 425 oz-in.

The other primary component of the jumping model is the shock absorber model. This model used for the shock absorber can be found in Fig. 5.4. The model consists of two bodies that comprise the shock absorber and a revolute joint that allows the shock rotate about its end point. As the shock absorber has a check valve that creates no damping during its return stroke, the only relevant dynamics of the shock absorber during jumping maneuvers is the energy added to the system by the relatively weak return spring. This is modeled with a simple gain value being multiplied on the position of the shock absorber end with the gain value being derived from the maximum return spring force listed in the shock absorber data sheet.

5.3 Falling Model

The second Simscape model produced was the falling model. The purpose of this model was to analyze the final maximum fall height after implementing the attached passive elements as well as the shock absorber. The model features two stages. In the first stage, the leg is pushed up to the test fall height. The model sits at that height until it is dropped and allowed to fall toward the ground where it collides with the ground and slowed to a stop by the actuators and shock absorber. The full model can be found in Fig. 5.5.

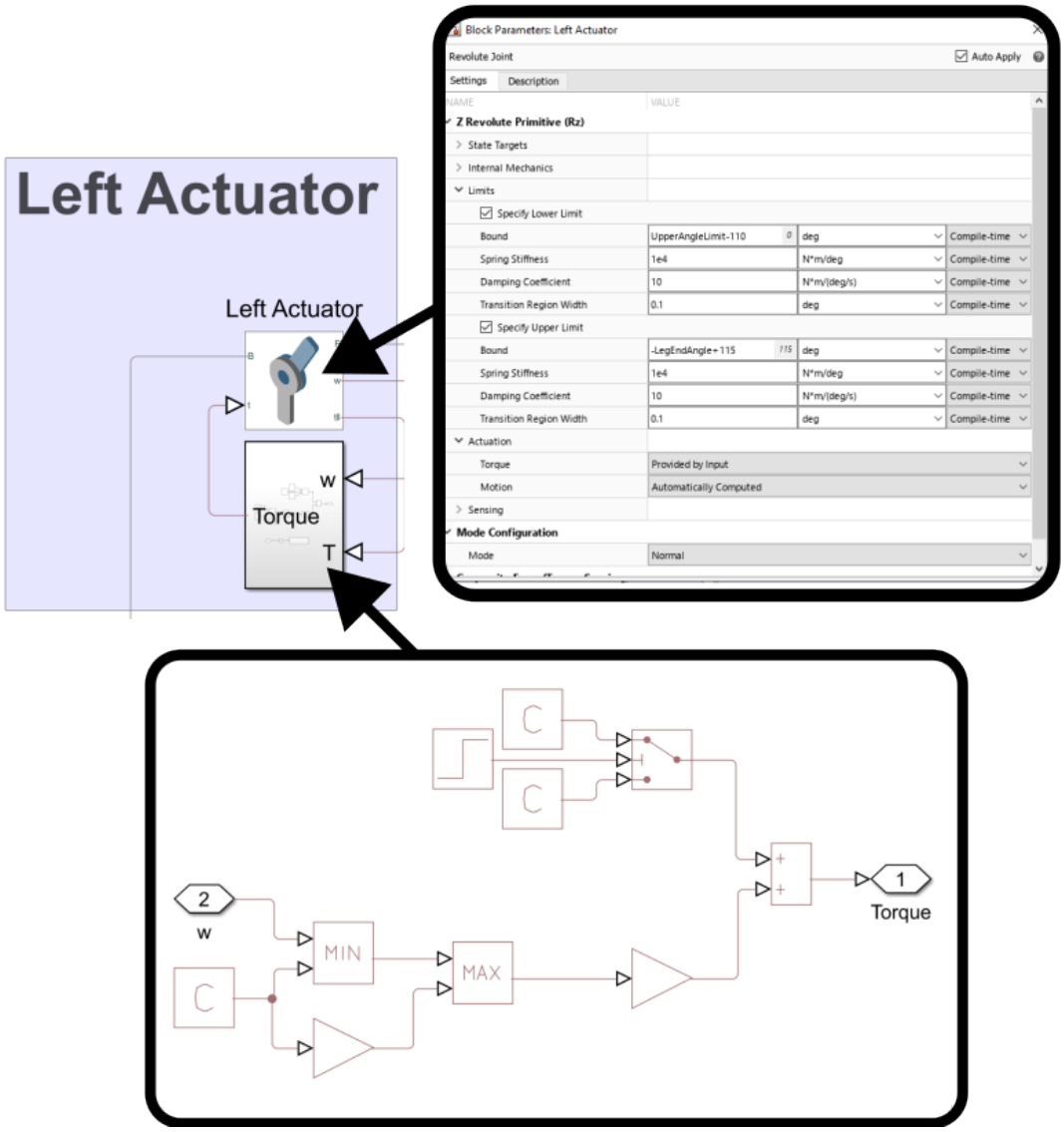

Figure 5.3: Jumping simulator actuator model.

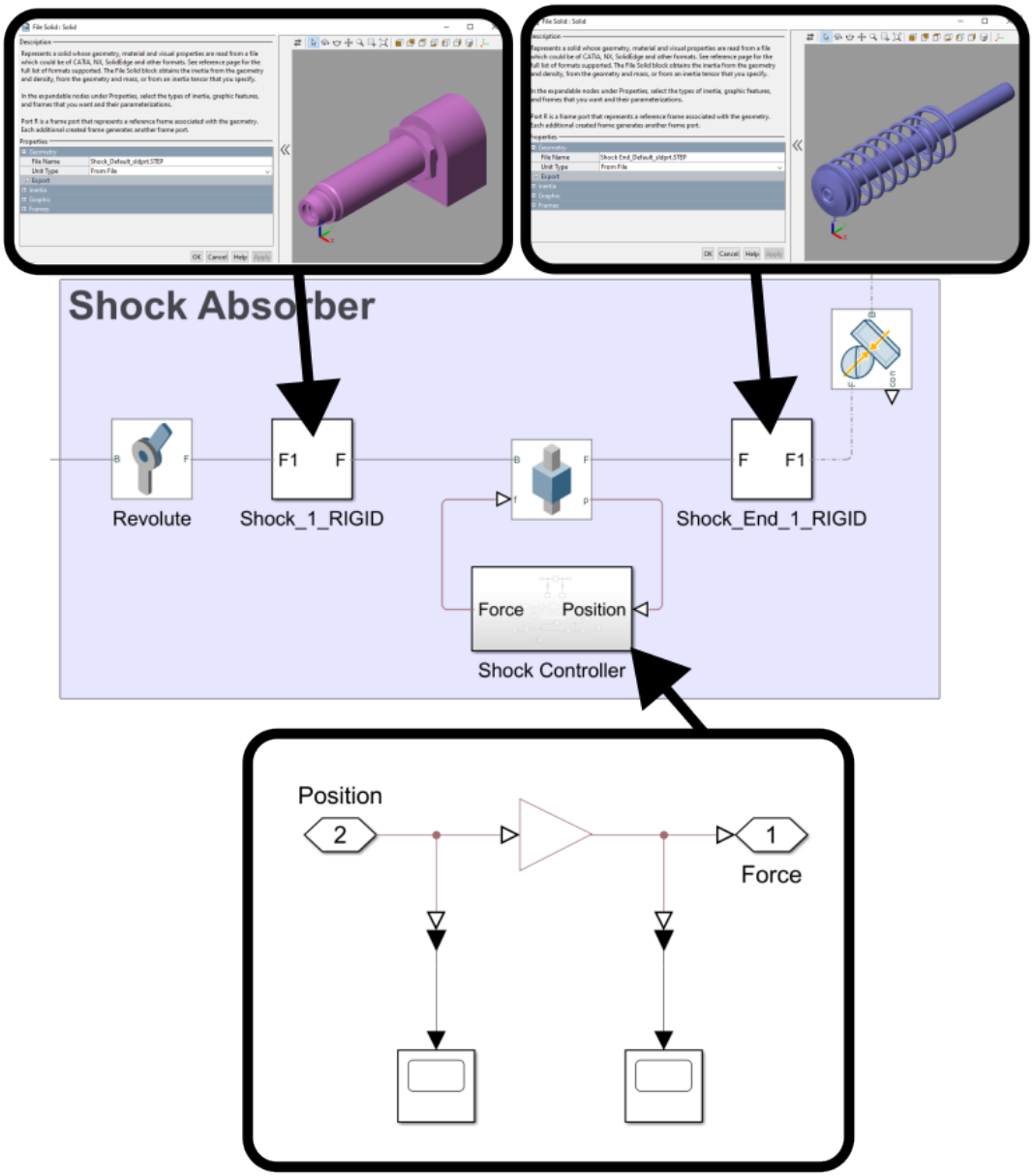

Figure 5.4: Jumping simulator shock absorber model.

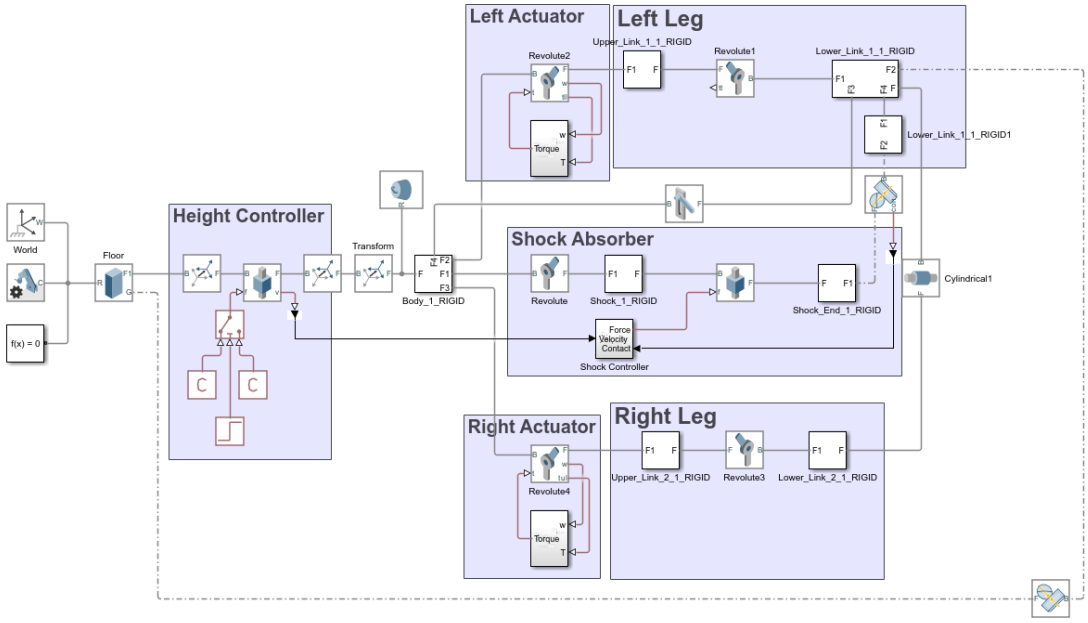

Figure 5.5: Falling simulator full model.

Unlike the jumping model, the fall model features its two stage behavior in the height controller instead of within the actuator although the working principle is the same. The prismatic joint that governs the degrees of freedom for the height of the leg has a maximum length set at the desired test height. Then a force is applied to lift the system to this height until it switches to applying zero force and the leg is allowed to fall. The actuator for this model does not feature the switching as seen in the jumping simulator and instead applies a constant motor torque pushing the leg into the extended configuration in additional to the same damper model implemented in the jumping simulation.

Other than the jump height simulator, the other major change in this model is the implementation of the shock absorber. The shock absorber model can be found in Fig. 5.6. Instead of implementing the return spring as was done in the jumping model, this shock absorber model implements the force curve response that an ideal shock absorber produces. Specifically, this shock absorber model produces a force to counteract the velocity that the shock absorber experiences on contact with the foot. This is done by measuring the velocity of the body at the instant that the shock end contacts the foot as read from the foot-shock spacial contact block. It then calculates the kinetic energy the system has and outputs a constant force over the length of the shock to completely dis-

sipate the kinetic energy. Additionally, it only applied this force while both the velocity is negative and the foot is in contact with the shock end.

5.4 Damper Solver Model

The model used to solve for the effectively linear spring constant and the effective linear damping constant is almost identical to the model used to test the legs maximum fall height. However, for this model, the height is set at a constant value and instead a positional input is set into the pin joint that governs the motion of the foot as seen in Fig. 5.7. When using this model to solve for the effective linear spring constant, the damping value is set to zero and the force required to push the foot vertically as governed by the ramp input is recorded. Once the effective linear spring constant is calculated, the knee spring value is set to zero and a test damping value is set. Again the foot is pushed upward and the force is recorded. This force recording is then compared to the force required to push the foot with both a spring constant of zero and a damping constant of zero to determine the force being added by the damper.

5.5 Torque Solver Model

To solve for the torques required by the actuators to complete a single gait cycle the model found in Fig. 5.8 was used. The model uses a simplified leg model that does not implement the CAD model as the added details provided by the CAD model would not impact the final energy calculations. The model functions by providing the foot with a path to follow and the actuators producing the torque required to move the foot along the path. Sin waves are used in the path generator to remove discontinuities along the path that caused high impulse torques to be generated.

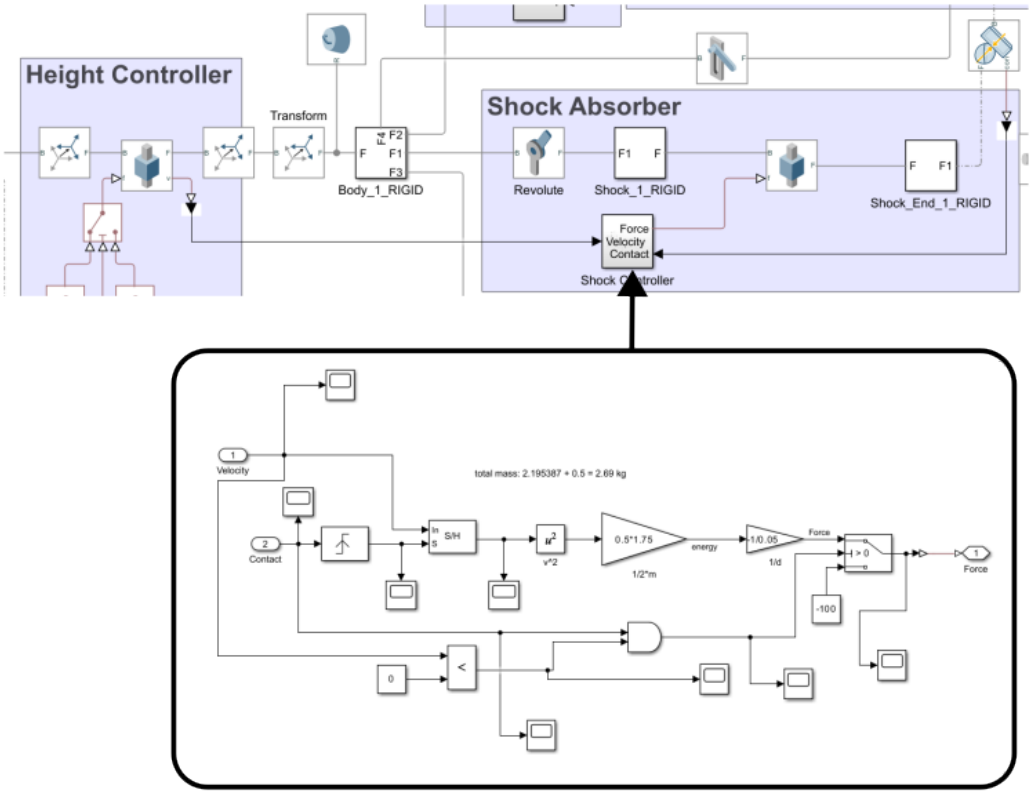

Figure 5.6: Falling simulator shock absorber model.

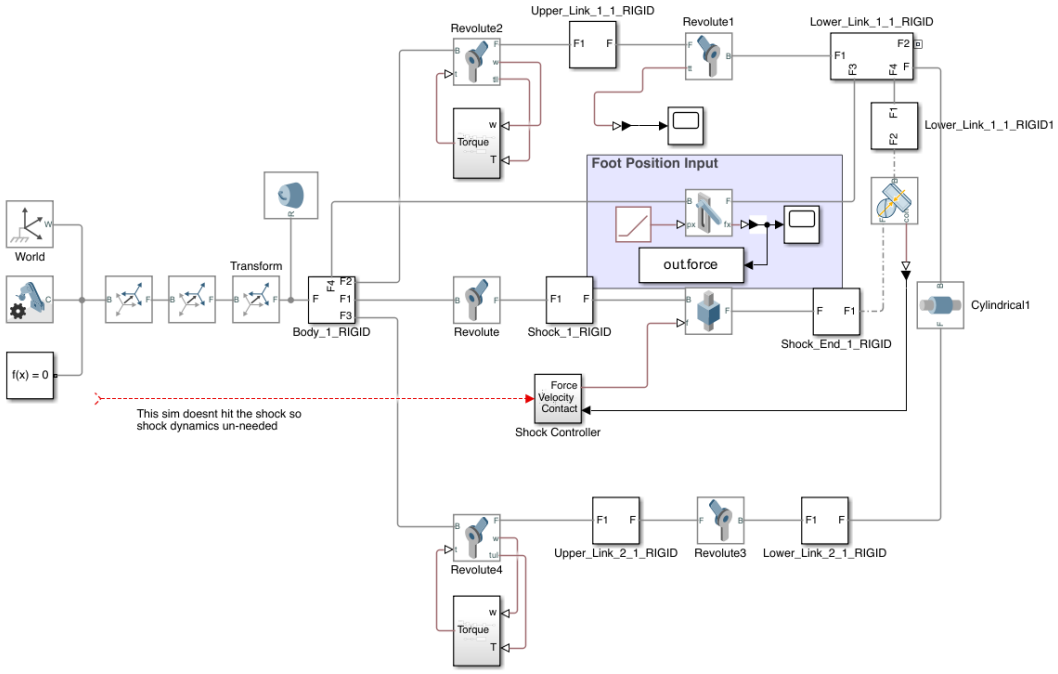

Figure 5.7: Damper analysis model.

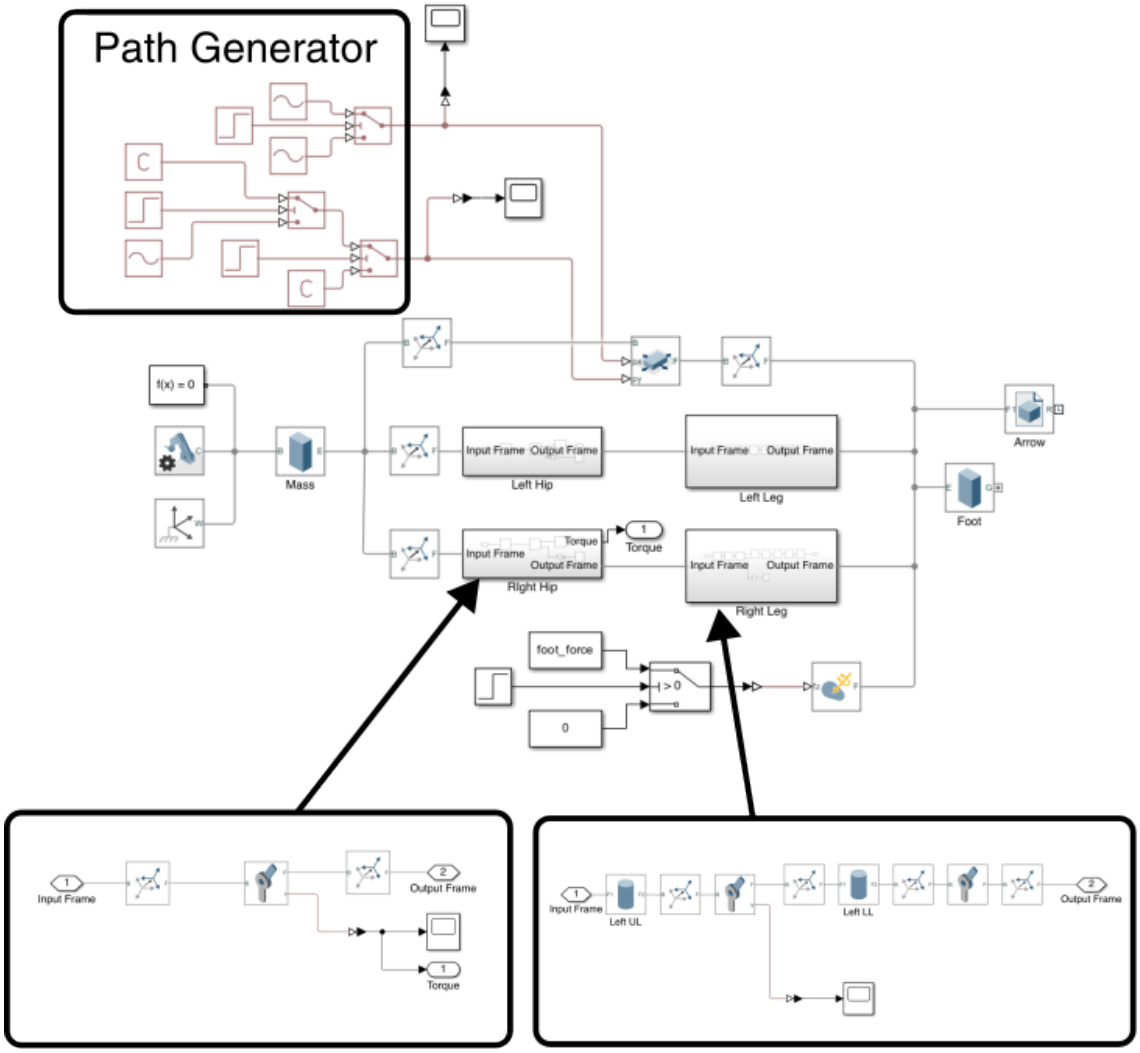

Figure 5.8: Torque analysis model.

Chapter 6

Results

Using the falling and jumping models developed in Chapter 5, the results for the BPE leg design was simulated. In this chapter these results will be discussed.

6.1 Falling Simulation

The falling simulation is used to determine the maximum height that the leg can fall. This is done by measuring the shock absorber impact velocity and verifying that it does not exceed the maximum shock absorber impact velocity. In Fig. 6.1, we can see the leg falling from a 6 meter height and impacting the ground. Using the the shock absorber controller, we can find the velocity that the shock absorber was impacted at. The impact velocity was measured at 4.34 m/s. This value is approximately the maximum impact velocity for the shock absorber for this systems impact energy making it the maximum fall height this design can sustain. Using the model, other simulation variables such as actuator torques, ground reaction forces, and joint positions can be extracted.

In the torque vs time graph found in Fig. 6.2, there are three distinct fluctuations in the actuator torques. The first of these fluctuations is cause by the leg moving from its initialization position to its fully extended position that is used during falling maneuvers. The second of these fluctuations occurs when the leg impacts the top of the prismatic joint which has its upper limit placed at the desired test fall height. The third and largest of these is at the impact of the leg with the ground. These fluctuations can also be found in Fig. 6.4, as the three position fluctuations are directly related to the torque fluctuations. This is due to the torque only being modified from its constant value of 8.3 Nm by the damper applying an additional torque, which only occurs when the leg output changes position. The final result found from this model is the GRF plot found in Fig.

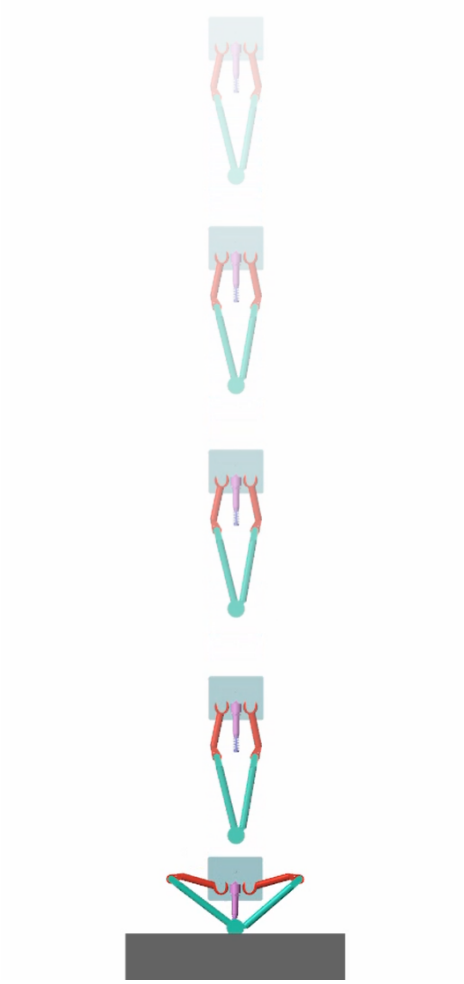

Figure 6.1: Falling simulation motion diagram.

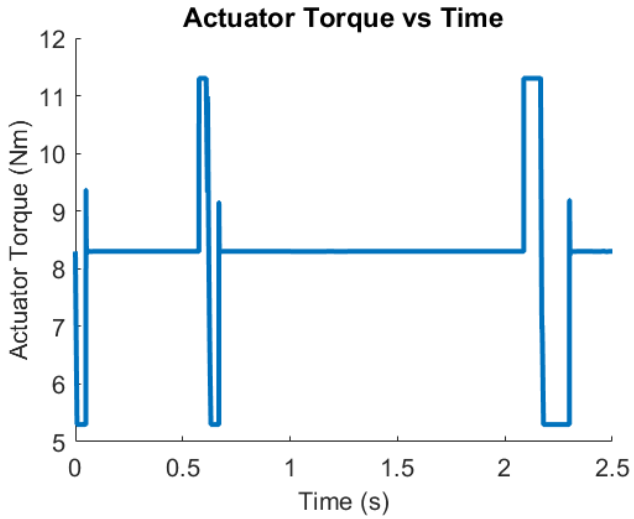

Figure 6.2: Falling simulation actuator torque vs time graph.

6.3. Figure 6.3a shows the magnitude of the impact impulse force topping 10,000 N. Figure 6.3b shows the GRF as a result of the actuator torques and and the shock absorber. Before the shock absorber engages, the GRF is around 100 N however, once the shock absorber makes contact and the majority of the work to slow down the leg is done, the GRF peaks at over 700 N.

6.2 Jumping Simulation

The jumping simulation is used to determine the maximum height that the leg can jump to. This is done by measuring the position leg support plate over a single jump. The final jump height is measured from the position at the legs most compressed position to the jump apex. In Fig. 6.5, we can see the leg jumping from a crouched position to over 0.93 m. In Fig. 6.6, the position of the leg support plate is plotted over time. We can see the apex of the jump height labelled and the minimum body position of the leg being set on the x-axis making the labelled apex equivalent to the maximum jump height. Using the model, other simulation variables such as actuator torques, ground reaction forces, and joint positions can be extracted.

In the torque vs time graph found in Fig. 6.7, the time in which the actuator model switches from compressing the leg to extending the leg can be clearly seen to occur at one second into the simulation time. Additionally, we can see how the damper reduces the effective output torque of the actuator from 8.3 Nm to around 5.3 Nm during the jumping motion. The actuator only begins producing an output torque of 8.3 Nm once the leg has reached the fully extended position

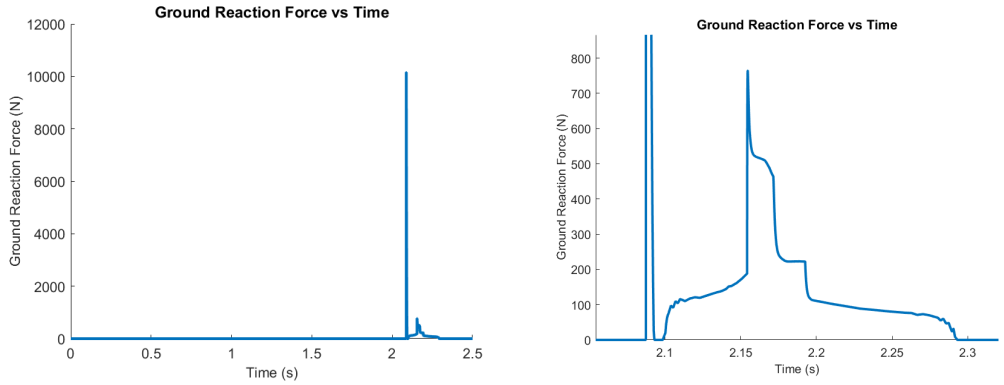

(a) Full graph. (b) Graph zoomed in on impact time.

Figure 6.3: Falling simulation GRF vs time.

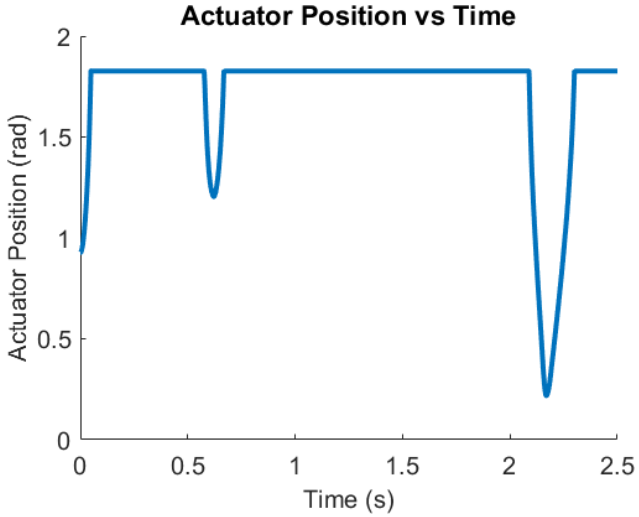

Figure 6.4: Falling simulation actuator position vs time graph.

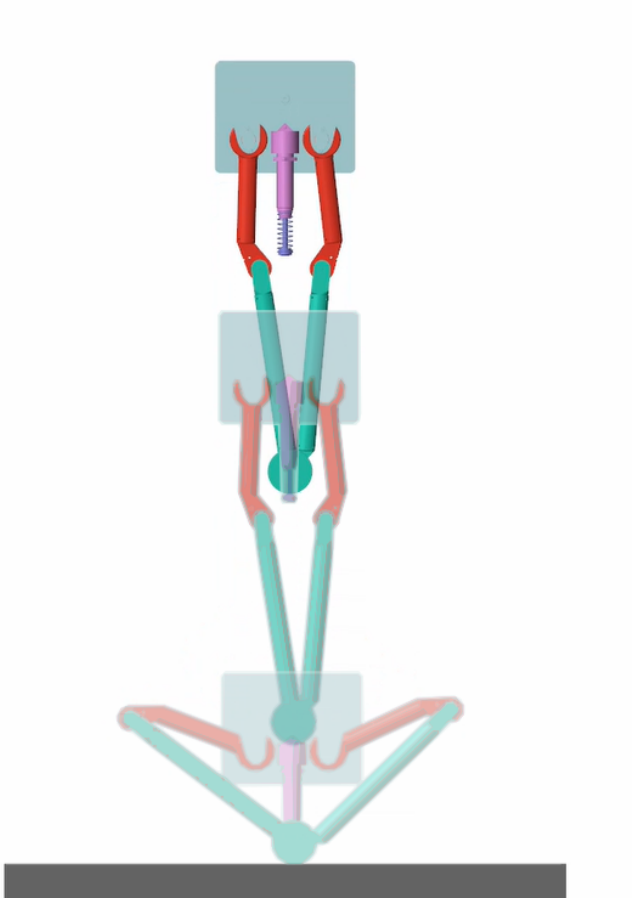

Figure 6.5: Jumping simulation motion diagram.

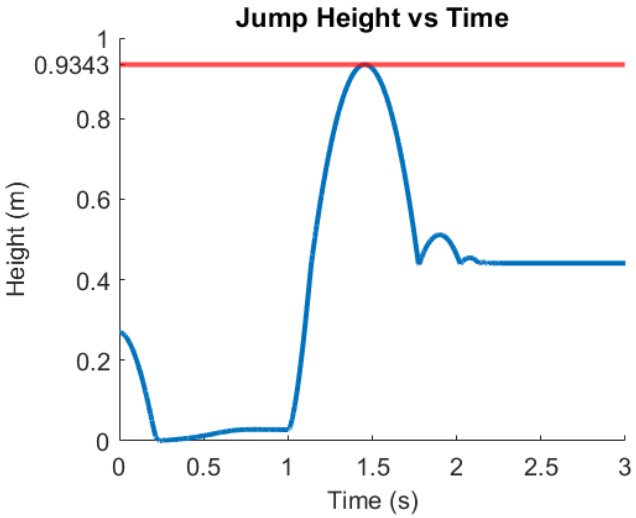

Figure 6.6: Jumping simulation body position vs time graph.

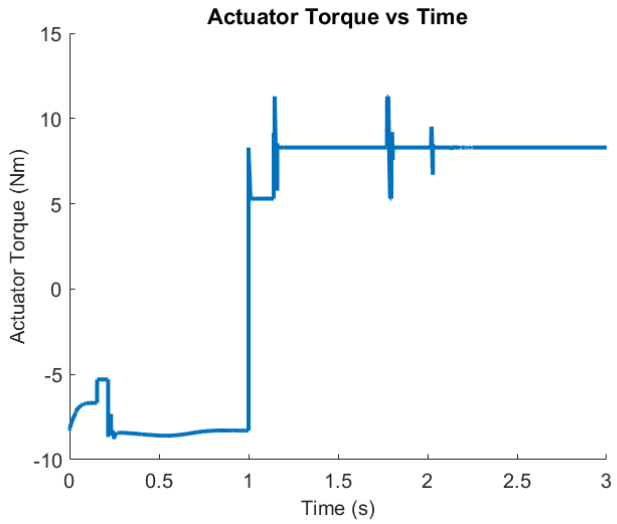

Figure 6.7: Jumping simulation actuator torque vs time graph.

and the rotational velocity goes to zero as seen in Fig. 6.9. The final result is the GRF vs time graphs found in Fig. 6.8. Figure 6.8a shows the GRFs for the full simulation duration. In this graph, the leg can be seen to bounce multiple times on landing, however, the magnitude of the impulse forces on each bounce make it hard to read the GRFs generated during the jump. Figure 6.8b shows the GRFs generated during the jumping maneuver by zooming in past the impulse force. We can see that as the actuator switches torque direction the GRF spikes but decreases as the main body accelerates. After the leg has lifted off the ground, we can see the GRFs drop to zero.

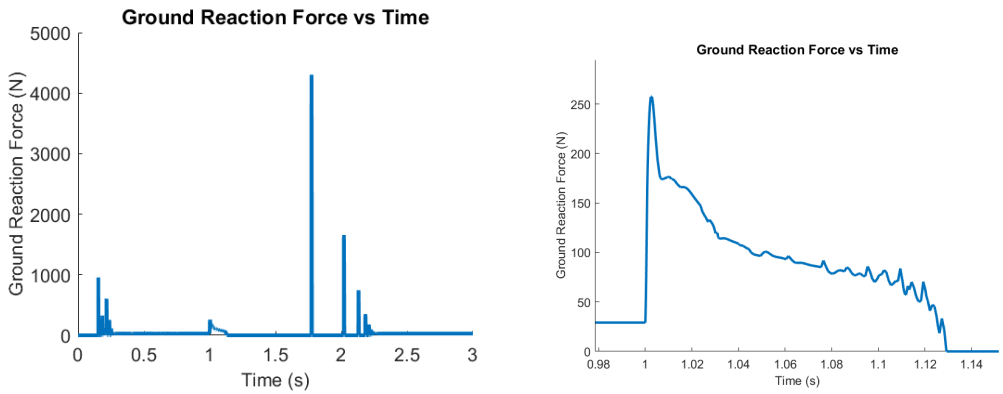

(a) Full graph, (b) Graph zoomed in on jump time.

Figure 6.8: Jumping simulation GRF vs time graph.

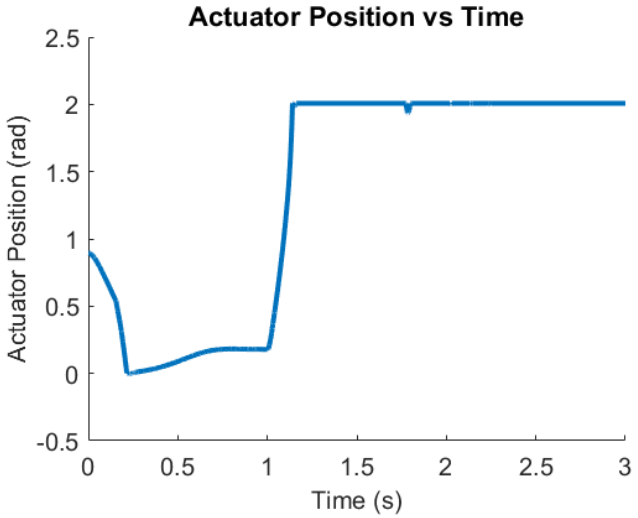

Figure 6.9: Jumping simulation position vs time graph.

Chapter 7

Conclusion

Using the framework I have created in this thesis, a binary passive element leg can be specified, analyzed, and then designed. In this thesis, I have justified the rational for designing a leg using the BPE model and parallel kinematics and how these foundations lead to improved leg characteristics such as robustness, fall dissipation, and agility. Next, using the framework I have laid out in this thesis for variable selection, the system parameters can be tuned to meet design objectives while balancing energy costs. The variable selection framework first discusses how to choose kinematic dimensions to ensure design objectives such as maximum gait and maximum actuator displacement are met. Next, it discusses how to choose a knee spring constant to increase standable task space area and how to find the energy costs of adding a knee spring, allowing the designer to balance standable area and increased energy consumption. Finally, it lays out a process for determining linear system constants for a two dimensional system and how these constants can be used to calculate the attached damping value to improve system robustness. In additional to laying out the theory for the variable selection analysis, I also applied this framework to design a BPE leg for Northeastern's Harpy platform.

With system variables chosen, I created hardware solutions for implementing the parallel kinematics and system constants determined using the variable selection framework. This includes designs for the four major subsystems of the leg. The first of these is an actuator design that implements a BLDC motor, harmonic drive, encoder, and a passive damper. Next, a knee joint was designed to implement an elastic element and pulley system to replicate the desired torsional spring constant. Finally, the foot and shock absorber designs implement features to ensure proper foot-shock interfacing and produce the slacked passive component behavior that the BPE model implements. As was done with the variable selection, I also created CAD for a BPE leg design for

Northeasterns's Harpy platform. The final contribution of this thesis is various Simulink models used to analyse the performance of the designed BPE leg. A falling model was developed to determine the maximum height that the leg can fall from without exceeding the limits of the shock absorber. Additionally, a jumping model was developed to determine the maximum height that the leg can jump.

7.1 Future Work

With the completion of this thesis there are three areas of the BPE leg design that require additional development. The first of these is performing an analysis derived from the work done in the paper "A little damping goes a long way" for the BPE model. This could be used to quantify and improve the attached dampers impact on robustness for the BPE model specifically. Next, the shock absorber curved extrusion may be improved by performing analysis on what curve shape is most effective on engaging the shock absorber end and ensuring proper foot shock alignment. Lastly, the limiting factor for maximum fall height is the shock absorber impact velocity. In the future, a custom shock absorber could be developed that is able to handle higher impact velocities at lower cycle energies, thus increasing the legs maximum fall height. In addition to these listed improvements that can be made to the current BPE leg design, future work could focus on increasing the number of element stages or implementing variable passive elements such as voltage controlled dampers. This could decrease the energy costs of current BPE passive elements while improving and expanding leg design objectives.

Bibliography

[1] M. Hutter, C. Gehring, D. Jud, A. Lauber, C. D. Bellicoso, V. Tsounis, J. Hwangbo, K. Bodie, P. Fankhauser, M. Bloesch, R. Diethelm, S. Bachmann, A. Melzer, and M. Hoepflinger, "ANYmal - a highly mobile and dynamic quadrupedal robot," in *2016 IEEE/RSJ International Conference on Intelligent Robots and Systems (IROS)*, Oct. 2016, pp. 38–44, iSSN: 2153-0866. [Online]. Available: https://ieeexplore.ieee.org/abstract/document/7758092

[2] C. G. Hobart, A. Mazumdar, S. J. Spencer, M. Quigley, J. P. Smith, S. Bertrand, J. Pratt, M. Kuehl, and S. P. Buerger, "Achieving Versatile Energy Efficiency With the WANDERER Biped Robot," *IEEE Transactions on Robotics*, vol. 36, no. 3, pp. 959–966, Jun. 2020. [Online]. Available: https://ieeexplore.ieee.org/document/9006922

[3] M. H. Raibert, *Legged Robots that Balance*. MIT Press, 1986, google-Books-ID: EXRiBnQ37RwC.

[4] M. Ahmadi and M. Buehler, "Preliminary experiments with an actively tuned passive dynamic running robot," in *Experimental Robotics V*, A. Casals and A. T. de Almeida, Eds. Berlin, Heidelberg: Springer, 1998, pp. 312–324.

[5] S. Kitano, S. Hirose, A. Horigome, and G. Endo, "TITAN-XIII: sprawling-type quadruped robot with ability of fast and energy-efficient walking," *ROBOMECH Journal*, vol. 3, no. 1, p. 8, Mar. 2016. [Online]. Available: https://doi.org/10.1186/s40648-016-0047-1

[6] W. C. Martin, A. Wu, and H. Geyer, "Experimental Evaluation of Deadbeat Running on the ATRIAS Biped," *IEEE Robotics and Automation Letters*, vol. 2, no. 2, pp. 1085–1092, Apr. 2017. [Online]. Available: https://ieeexplore.ieee.org/abstract/document/7833179

[7] P. Dangol, E. Sihite, and A. Ramezani, "Control of Thruster-Assisted, Bipedal Legged Locomotion of the Harpy Robot," *Frontiers in Robotics and AI*, vol. 8, Dec. 2021,

publisher: Frontiers. [Online]. Available: https://www.frontiersin.org/articles/10.3389/frobt.2021.770514

[8] S. Pitroda, "Dynamic Multimodal Locomotion: A Quick Overview of Hardware and Control," Master's thesis, Northeastern University, United States – Massachusetts, 2023, iSBN: 9798380156141. [Online]. Available: https://www.proquest.com/docview/2859376203/abstract/A276BA2F301345E1PQ/1

[9] P. Kelly, "Design of a thruster-assisted bipedal robot," 2021. [Online]. Available: https://repository.library.northeastern.edu/files/neu:bz60w8418

[10] A. Coffey, "Avoid a shock to the system," Jun. 2013. [Online]. Available: https://www.powermotiontech.com/hydraulics/reservoirs-accessories/article/21883175/avoid-a-shock-to-the-system

[11] "Non-Adjustable Series Hydraulic Shock Absorbers." [Online]. Available: https://airinc.net/wp-content/uploads/2018/12/Enidine_ECO-Series.pdf

[12] S. Rezazadeh, A. Abate, R. L. Hatton, and J. W. Hurst, "Robot Leg Design: A Constructive Framework," *IEEE Access*, vol. 6, pp. 54 369–54 387, 2018. [Online]. Available: https://ieeexplore.ieee.org/document/8466587

[13] M. Grimmer, M. Eslamy, S. Gliech, and A. Seyfarth, "A comparison of parallel- and series elastic elements in an actuator for mimicking human ankle joint in walking and running," in *2012 IEEE International Conference on Robotics and Automation*, May 2012, pp. 2463–2470, iSSN: 1050-4729. [Online]. Available: https://ieeexplore.ieee.org/abstract/document/6224967

[14] J. Chen, Z. Liang, Y. Zhu, C. Liu, L. Zhang, L. Hao, and J. Zhao, "Towards the Exploitation of Physical Compliance in Segmented and Electrically Actuated Robotic Legs: A Review Focused on Elastic Mechanisms," *Sensors*, vol. 19, no. 24, p. 5351, Jan. 2019. [Online]. Available: https://www.mdpi.com/1424-8220/19/24/5351

[15] T. Verstraten, P. Beckerle, R. Furnémont, G. Mathijssen, B. Vanderborght, and D. Lefeber, "Series and Parallel Elastic Actuation: Impact of natural dynamics on power and energy consumption," *Mechanism and Machine Theory*, vol. 102, pp. 232–246, Aug. 2016. [Online]. Available: https://www.sciencedirect.com/science/article/pii/S0094114X16300301

[16] G. Mathijssen, B. Brackx, M. Van Damme, D. Lefeber, and B. Vanderborght, "Series-parallel elastic actuation (SPEA) with intermittent mechanism for reduced motor torque and increased efficiency," in *2013 IEEE/RSJ International Conference on Intelligent Robots and Systems*, Nov. 2013, pp. 5841–5846, iSSN: 2153-0866. [Online]. Available: https://ieeexplore.ieee.org/document/6697202

[17] S. Heim, M. Millard, C. Le Mouel, and A. Badri-Spröwitz, "A little damping goes a long way: a simulation study of how damping influences task-level stability in running," *Biology Letters*, vol. 16, no. 9, p. 20200467, Sep. 2020. [Online]. Available: https://royalsocietypublishing.org/doi/10.1098/rsbl.2020.0467

[18] P. M. Wensing, A. Wang, S. Seok, D. Otten, J. Lang, and S. Kim, "Proprioceptive Actuator Design in the MIT Cheetah: Impact Mitigation and High-Bandwidth Physical Interaction for Dynamic Legged Robots," *IEEE Transactions on Robotics*, vol. 33, no. 3, pp. 509–522, Jun. 2017. [Online]. Available: https://ieeexplore.ieee.org/document/7827048

[19] M. Ratiu and D. M. Anton, "A brief overview of parallel robots and parallel kinematic machines," *IOP Conference Series: Materials Science and Engineering*, vol. 898, no. 1, p. 012007, Jul. 2020. [Online]. Available: https://iopscience.iop.org/article/10.1088/1757-899X/898/1/012007

[20] M. Morisawa, T. Yakoh, T. Murakami, and K. Ohnishi, "A comparison study between parallel and serial linked structures in biped robot system," in *2000 26th Annual Conference of the IEEE Industrial Electronics Society. IECON 2000. 2000 IEEE International Conference on Industrial Electronics, Control and Instrumentation. 21st Century Technologies*, vol. 4, Oct. 2000, pp. 2614–2619 vol.4. [Online]. Available: https://ieeexplore.ieee.org/document/972410

[21] Y. Zhong, R. Wang, H. Feng, and Y. Chen, "Analysis and research of quadruped robot's legs: A comprehensive review," *International Journal of Advanced Robotic Systems*, vol. 16, no. 3, p. 172988141984414, May 2019. [Online]. Available: http://journals.sagepub.com/doi/10.1177/1729881419844148

[22] K. Liang, E. Sihite, P. Dangol, A. Lessieur, and A. Ramezani, "Rough-Terrain Locomotion and Unilateral Contact Force Regulations With a Multi-Modal Legged Robot," in *2021 American Control Conference (ACC)*, May 2021, pp. 1762–1769, iSSN: 2378-5861.

[23] A. Ramezani, P. Dangol, E. Sihite, A. Lessieur, and P. Kelly, "Generative Design of NU's Husky Carbon, A Morpho-Functional, Legged Robot," in *2021 IEEE International Conference on Robotics and Automation (ICRA)*, May 2021, pp. 4040–4046, iSSN: 2577-087X. [Online]. Available: https://ieeexplore.ieee.org/abstract/document/9561196

[24] A. Salagame, S. Manjikian, C. Wang, K. V. Krishnamurthy, S. Pitroda, B. Gupta, T. Jacob, B. Mottis, E. Sihite, M. Ramezani, and A. Ramezani, "A Letter on Progress Made on Husky Carbon: A Legged-Aerial, Multi-modal Platform," Jul. 2022, arXiv:2207.12254 [cs, eess]. [Online]. Available: http://arxiv.org/abs/2207.12254

[25] E. Sihite, A. Kalantari, R. Nemovi, A. Ramezani, and M. Gharib, "Multi-Modal Mobility Morphobot (M4) with appendage repurposing for locomotion plasticity enhancement," *Nature Communications*, vol. 14, no. 1, p. 3323, Jun. 2023, publisher: Nature Publishing Group. [Online]. Available: https://www.nature.com/articles/s41467-023-39018-y

[26] K. Kim, P. Spieler, E.-S. Lupu, A. Ramezani, and S.-J. Chung, "A bipedal walking robot that can fly, slackline, and skateboard," *Science Robotics*, vol. 6, no. 59, p. eabf8136, Oct. 2021, publisher: American Association for the Advancement of Science. [Online]. Available: https://www.science.org/doi/10.1126/scirobotics.abf8136

[27] P. Dangol and A. Ramezani, "Feedback design for Harpy: a test bed to inspect thruster-assisted legged locomotion," in *Unmanned Systems Technology XXII*, vol. 11425. SPIE, May 2020, pp. 49–55. [Online]. Available: https://www.spiedigitallibrary.org/conference-proceedings-of-spie/11425/1142507/Feedback-design-for-Harpy--a-test-bed-to-inspect/10.1117/12.2558284.full

[28] P. Dangol, A. Ramezani, and N. Jalili, "Performance satisfaction in Harpy, a thruster-assisted bipedal robot," *arXiv:2004.14337 [cs, eess]*, Apr. 2020, arXiv: 2004.14337. [Online]. Available: http://arxiv.org/abs/2004.14337

[29] P. Dangol and A. Ramezani, "Towards thruster-assisted bipedal locomotion for enhanced efficiency and robustness," *IFAC-PapersOnLine*, vol. 53, no. 2, pp. 10 019–10 024, Jan. 2020. [Online]. Available: https://www.sciencedirect.com/science/article/pii/S2405896320334844

[30] A. C. B. de Oliveira and A. Ramezani, "Thruster-assisted Center Manifold Shaping in Bipedal Legged Locomotion," in *2020 IEEE/ASME International Conference on Advanced Intelligent*

Mechatronics (AIM), Jul. 2020, pp. 508–513, iSSN: 2159-6255. [Online]. Available: https://ieeexplore.ieee.org/document/9158967

[31] "HDS® Fans Archives." [Online]. Available: https://www.schubeler.com/product-category/hds-fans/

[32] "CSF-GH & CSG-GH." [Online]. Available: https://www.harmonicdrivegearhead.com/technology/harmonic-drive

[33] "RMB20 Rotary Magnetic Encoder Module." [Online]. Available: https://www.rls.si/eng/rmb20-10

[34] "MN4006 Antigravity Type 4-6S UAV Motor kv380 - 2PCS/SET_antigravity Type_motors_uav Power_t-MOTOR Official Store - UAV Power System, Robot Power System, Model Power System." [Online]. Available: https://store.tmotor.com/goods.php?id=440